Summer 1987

# The Influence of Transverse Magnetic Fields on the Current-Voltage Characteristics of Glow Discharges

Thomas J. Powers
*Old Dominion University*

# THE INFLUENCE OF TRANSVERSE MAGNETIC FIELDS ON THE CURRENT-VOLTAGE CHARACTERISTICS OF GLOW DISCHARGES

by

Thomas J. Powers
B.S. in Electrical Engineering, May 1980
Old Dominion University

A Thesis Submitted to the Faculty of
Old Dominion University in Partial Fulfillment
of the Requirements for the Degree of

MASTER OF ENGINEERING

ELECTRICAL ENGINEERING

OLD DOMINION UNIVERSITY
Aug. 1987

Approved by:

Karl H. Schoenbach (Director)

Linda L. Vahala

V. Lakdawala

ABSTRACT

In low pressure discharges, operated in electronegative gas mixtures to the right of the Paschen curve minimum, the discharge resistance can be increased by application of transverse magnetic fields. In this range of operation, both the mean free path and the larmor radius are small compared to the discharge dimensions. The relationship between the electric field and the magnetic field is therefore controlled by electron-molecule collisional processes. Specifically, the magnetically induced increase in the discharge resistance is caused by a downward shift of the electron energy distribution which leads to an increase in attachment and a reduction in ionization.

In this work the effect of a transverse magnetic field on a glow discharge has been investigated. Measurements of the steady-state current-voltage characteristics of glow discharges in transverse magnetic fields have been performed in He and He/$SF_6$ gas mixtures. The experimental setup and diagnostics are described, and the experimental results are presented. The experimental results indicate an increase of discharge voltage in He/$SF_6$ mixture at 8 torr of 2.5 kV/Tesla. This is in good agreement with Monte Carlo calculations of the electric field intensity in the positive column.

ACKNOWLEDGMENTS

I would like to express my appreciation to Dr. Karl Schoenbach for his guidance and support on this project. I would also like to thank Drs. Linda Valahala and V. Lakdawala for reviewing this manuscript and being on my committee. I would like to thank Randy Cooper, who did the original theoretical calculations and experimental work. My thanks also go to Sung Ko and Mike Mazzola for their effort. Finally, I would like to thank my wife for her support and understanding during the course of this program.

TABLE OF CONTENTS

LIST OF TABLES

LIST OF FIGURES

## LIST OF SYMBOLS

| | |
|---|---|
| a | attachment rate coefficient |
| a | radial dimension (inner) of magnetic field coil |
| a | number of electrons in the swarm |
| a | radial dimension (inner) of a co-axial capacitor |
| A | amperes |
| A | constant for Aston Equations |
| A | area |
| A | the reciprocal of the divider ratio of the capacitive-resistive voltage divider |
| b | radial dimension (outer) of magnetic field coil |
| b | radial dimension (outer) of a co-axial capacitor |
| B | constant for Aston Equations |
| B | magnetic field intensity |
| $\underline{B}$ | magnetic field vector |
| B/N | reduced magnetic field intensity |
| $B_c$ | critical magnetic field intensity |
| $B_z$ | magnetic field intensity in the z-direction |
| C | Capacitance |
| $C_1$ | the center conductor-to-foil capacitance of the capacitive-resistive voltage divider |

| | |
|---|---|
| $C_2$ | the foil-to-outer conductor capacitance of the capacitive-resistive voltage divider |
| d | gap spacing |
| $d_{an}$ | cathode fall distance (abnormal glow) |
| $d_c$ | cathode fall distance |
| $d_n$ | cathode fall distance (normal glow) |
| E | electric field intensity |
| $\underline{E}$ | electric field vector |
| E | constant for Aston Equations |
| $E_o$ | electric field intensity at the cathode |
| $E_\theta$ | effective electric field |
| E/N | reduced electric field intensity |
| $(E/N)_e$ | effective reduced electric field intensity |
| F | constant for Aston Equations |
| h | length of the magnetic field coil |
| J | current density |
| $\underline{J}$ | current density (vector) |
| $J_o$ | primary current density |
| $k_a$ | attachment rate |
| $k_i$ | ionization rate |
| $k_r$ | recombination rate |
| kV | kilovolts |
| m | meters |
| $m_e$ | electron mass |
| M | ion or neutral mass |
| $n_e$ | electron number density |
| N | neutral particle number density |

| | |
|---|---|
| $N_a$ | attacher gas number density |
| $N_i$ | ionizing gas number density |
| $N_o$ | number density at 1 torr |
| p | pressure |
| P | power |
| R | positive column radius |
| $R_s$ | series damping resistor |
| $R_2$ | termination resistor in capacitive-resistive voltage divider |
| $R_1$ | series resistor in capacitive-resistive voltage divider |
| $T_e$ | electron temperature |
| Td | Townsend [1Td = $10^{17}$ V-cm] |
| T | pulse width |
| $\Delta t$ | time between samples |
| v | velocity |
| $v_e$ | electron velocity |
| $\underline{v}_e$ | electron velocity vector |
| $v_x$ | x-component of velocity |
| $v_{xo}$ | the initial value $v_x$ |
| $v_y$ | y-component of velocity |
| $v_{yo}$ | the initial value $v_y$ |
| $v_z$ | z-component of velocity |
| $v_{zo}$ | the initial value $v_z$ |
| $v_\perp$ | velocity component perpendicular to $\underline{B}$ |
| $V_{an}$ | cathode fall voltage (abnormal glow) |
| $V_d$ | discharge voltage |

| | |
|---|---|
| $V_n$ | cathode fall voltage (normal glow) |
| $V_o(s)$ | laplace transform of the input voltage ($v_o(t)$) |
| $V_2(s)$ | laplace transform of the output voltage ($v_2(t)$) |
| $X_i$ | the $i^{th}$ data point of a file |
| $X_n$ | the $n^{th}$ data point of a file |
| $x_o$ | the initial position in the x-direction |
| $y_o$ | the initial position in the y-direction |
| $z_g$ | total number of ion pairs |
| $z_o$ | the initial position in the z-direction |
| $z_{max}$ | the maximum distance traveled by an electron |
| $\alpha$ | ionization rate coefficient |
| $\delta$ | fractional energy lost in an elastic collision |
| $\varepsilon$ | permittivity of a material |
| $\kappa$ | average ionization coefficient |
| $\gamma$ | Townsend secondary emission coefficient |
| $\nu_c$ | collision frequency |
| $\mu_e$ | electron mobility |
| $\mu_{ex}$ | electron mobility in the x-direction |
| $\mu_o$ | magnetic permeability of free space |
| $\nu_o$ | normalized collision frequency |
| $\sigma_c$ | collision cross section |
| $\sigma$ | conductivity |
| $\eta$ | effective ionization rate |
| $\theta$ | effective electric field direction |
| $\tau$ | exponential decay time |
| $\omega_c$ | cylclotron frequency |

# Chapter I
# INTRODUCTION AND BACKGROUND

## The Glow Discharge

Glow discharges are electrical discharges in a gaseous medium which are characterized by a low degree of ionization and an electron temperature that is much greater than that of the gas molecules or ionic species. They are usually operated at low pressures and with current densities on the order of 10 $mA/cm^2$ [1]. In this section, the general characteristics of a glow discharge will be discussed and empirical equations for the voltage-current relationship and the current-geometry relationship will be introduced. The electrical characteristics of a glow discharge are shown in Figure 1. These characteristics may be broken down into several different regions whose description follows [2,3,4].

The Townsend dark discharge: This region is characterized by a discharge voltage on the order of 1000 $V_{dc}$ and currents in the range of $10^{-12}$ to $10^{-5}$ A. The voltage across the discharge remains relatively constant over this range of currents. In this range primary electrons are generated at the cathode by thermionic, field and photo emission. These electrons are accelerated by the electric field and

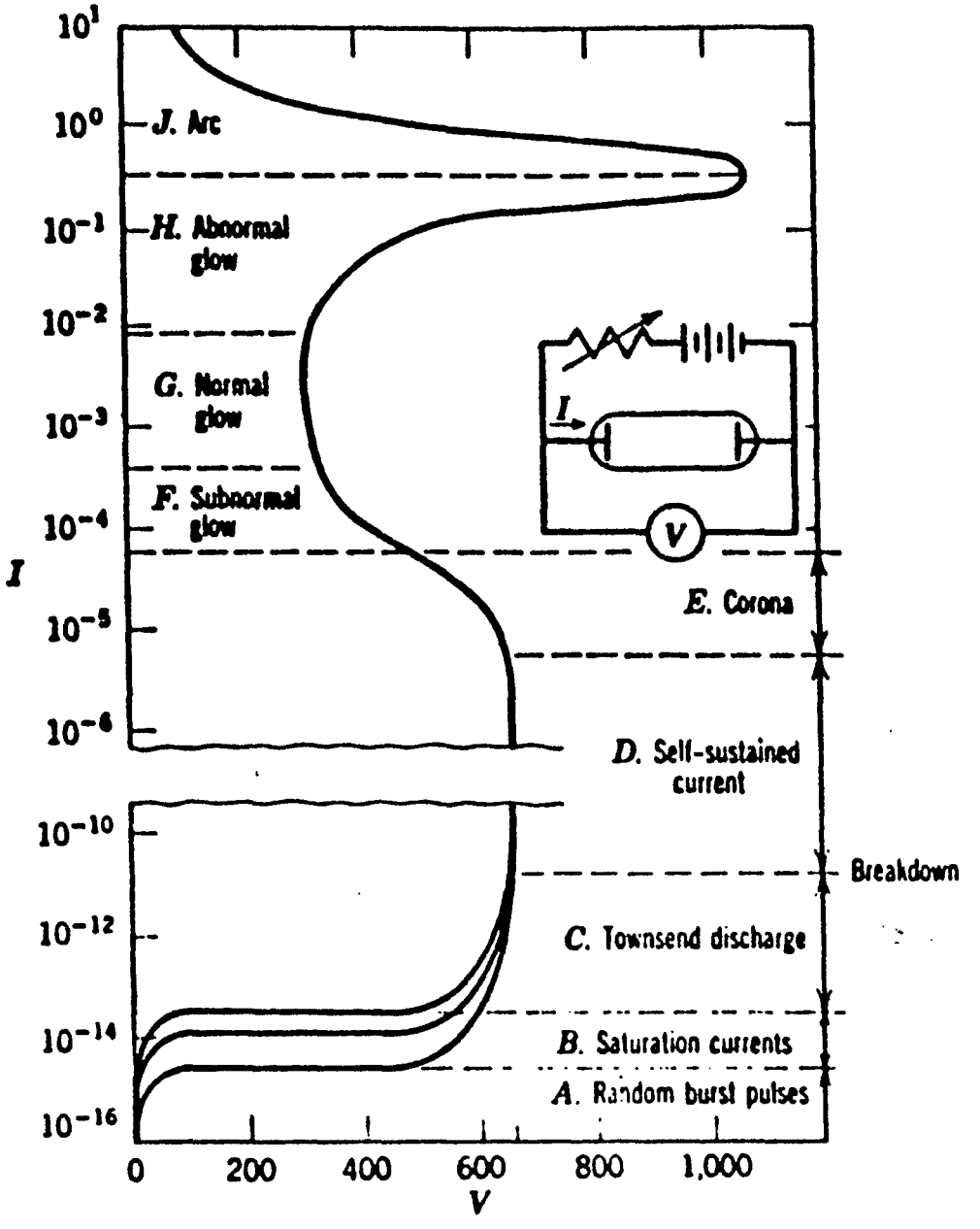


Figure 1. Voltage-Current characteristics of a glow discharge [2].

have ionizing collisions with the gas molecules. The ions are accelerated back to the cathode and secondary electron emission occurs. The electric field intensity is constant, and the discharge is not self-sustaining. Prior to this range the discharge is characterized by random pulses of $10^{-16}$ A peak.

Self-sustained discharge: In this region the discharge is self sustaining. This means that prior to the discharge becoming a self-sustained discharge there must be some type of primary emission process (e.g. external photo-ionization etc.) occurring at the cathode to maintain the discharge. The current can vary by several orders of magnitude with only a slight change in the discharge voltage.

Subnormal glow discharge: In this region the current rises while the voltage drops (e.g., negative differential conductivity). Additionally, space charges have a larger effect on the electric field distribution, and the different regions (cathode fall, negative glow and positive column) of the discharge are formed.

Normal glow discharge: The discharge in this range is stratified into several layers which vary in optical emission intensity and charge density. At the lower range of currents the cathode is only partially covered with a glow discharge. As the current increases the voltage across the discharge, $V_n$,

remains constant (on the order of 200 volts) and more of the cathode is covered by the glow until the entire cathode is covered. At this time the discharge voltage increases and the discharge is changing to an abnormal glow discharge.

Abnormal glow discharge: In this region the discharge is characterized by an exponential rise in voltage with respect to current. This rise is due to the increased cathode current density which can only be maintained by increasing the electric field in the the cathode fall region. Both the normal and abnormal glow voltages are proportional to $j/p^2$ where j is the current density and p is the gas pressure [5]. Additionally, the cathode fall distance decreases with increasing current density which further increases the electric field. In this range of operation the gas temperature in the cathode fall increases [6].

Glow to arc transition: In this region the discharge transitions from a diffuse glow discharge to an intense arc discharge which has a typical "on" voltage on the order of ten volts and high current densities.

A Normal glow discharge is stratified into several regions (spatial) which may be distinguished by their relative brightness. These regions along with the electric field intensity, luminous intensity, potential, space charge density and current density are shown in

Figure 2. The discharge may be divided into four major regions; the cathode fall, negative glow - faraday dark space, positive column and the anode region. In addition to the relative brightness of these layers each is characterized by specific electron molecule interaction processes.

The layers of the discharge near the cathode are the Aston dark space, cathode layers, and the cathode (Crooks) dark space. These layers are known as the cathode fall region. In this region the primary component of current flow is ion current, vice electron current which is dominant in the remainder of the discharge. For short discharges, the majority of the voltage across the discharge is across this region. Electrons gain high energies in this region.

Electrons with energies uniformly distributed from zero to typically 12 electron-volts [7,8] are introduced into the discharge from the cathode. These electrons are generated primarily by ionic secondary emission. However, they might also be generated by thermionic emission, photo emission and secondary emission caused by neutral molecules. Thermionic processes are important in hot cathode tubes and photo emission is important in devices driven by radioactive sources. Secondary emission by neutral molecules becomes more important at elevated current densities (which cause higher ion temperatures) because the ion - neutral cross section becomes larger at

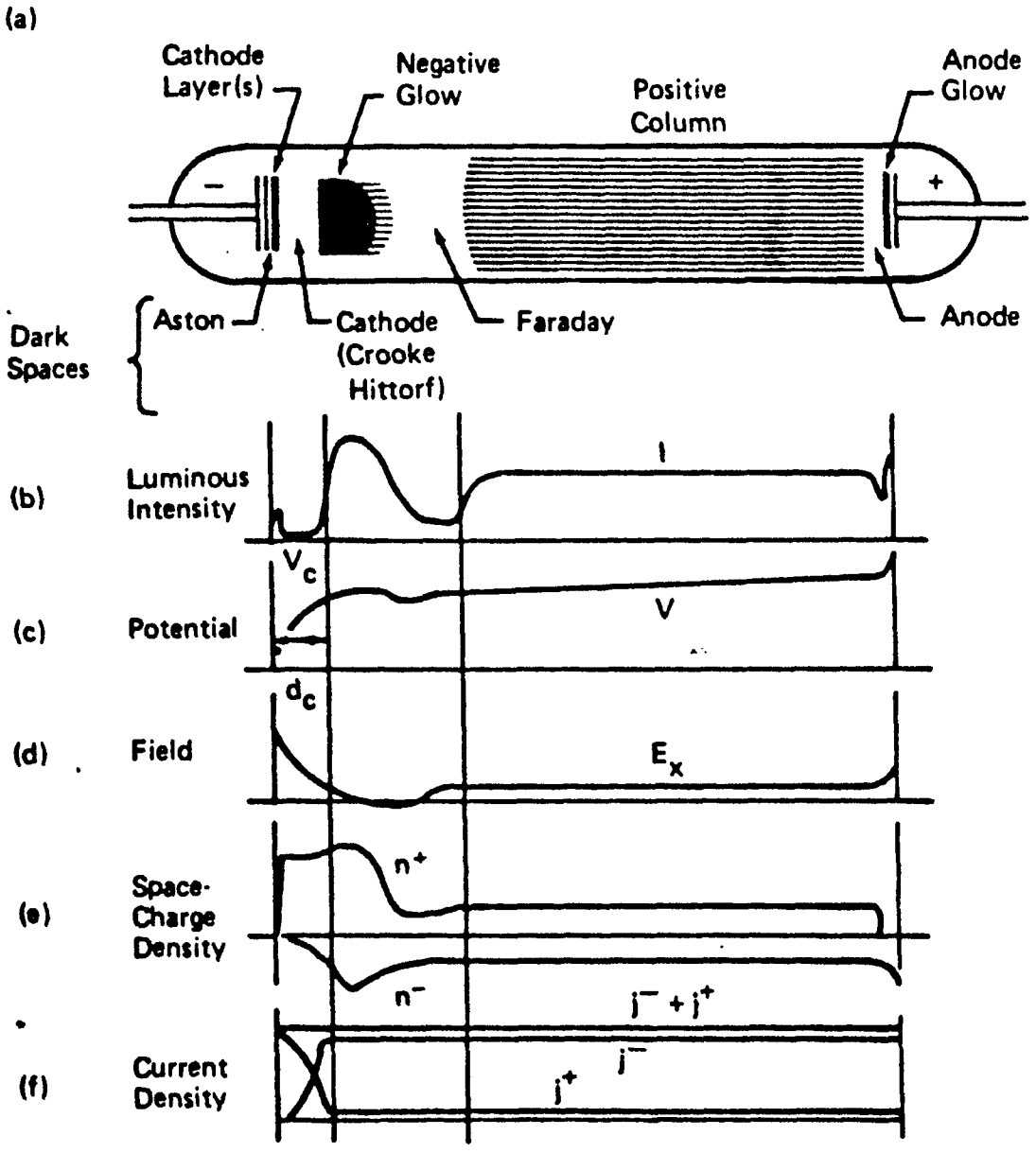


Figure 2. Glow discharge characteristics; (a) common names of the regions, (b) luminous intensity, (c) potential, (d) electric field intensity, (e) space-charge density, (f) current density [2].

larger ion energies [9]. Due to their low velocity, the emitted electrons cause a build up of negative space charge near the cathode, also - in electronegative gases - these low energy electrons have a relatively high probability of attachment near the cathode which would further increase this negative space charge. The electrons are accelerated by the electric field and the probability of attachment decreases and that of excitation or ionization increases. This process continues until the electrons reach the boundary of the negative glow.

The length of the normal cathode fall region, $d_c$, is inversely proportional to the pressure. The pressure-distance product $p \cdot d_c$ is of the same order of magnitude for different gases. Table I contains values of $pd_c$ (cm-torr) for several cathode materials and gas types.

Table I, values of $pd_c$ (cm.Torr) [2]

| Cathode | Air | A | $H_2$ | He | Ng | $N_2$ | Ne | $O_2$ |
|---|---|---|---|---|---|---|---|---|
| Al | 0.25 | 0.29 | 0.72 | 1.32 | 0.33 | 0.31 | 0.64 | 0.24 |
| C | .... | .... | 0.9 | .... | 0.69 | 1 | .... | .... |
| Cd | .... | .... | 0.87 | .... | .... | .... | .... | .... |
| Cu | 0.23 | .... | 0.8 | .... | 0.6 | .... | .... | .... |
| Fe | 0.52 | 0.33 | 0.9 | 1.30 | 0.34 | 0.42 | 0.72 | 0.31 |
| Hg | .... | .... | 0.9 | .... | .... | .... | .... | .... |
| Mg | .... | .... | 0.61 | 1.45 | .... | 0.35 | .... | 0.25 |
| Ni | .... | .... | 0.9 | .... | 0.4 | .... | .... | .... |
| Pb | .... | .... | 0.84 | .... | .... | .... | .... | .... |
| Pt | .... | .... | 1.0 | .... | .... | .... | .... | .... |
| Zn | .... | .... | 0.8 | .... | .... | .... | .... | .... |

As the discharge transitions to an abnormal glow the cathode fall distance, $d_{an}$, decreases and the cathode

fall voltage, $V_{an}$, increase in agreement with the following empirical equations (for plane electrodes) [3].

$$d_{an} = A/p + B/(j)1/2 \quad (1)$$

$$V_{an} = E + [F \times (j)^{1/2}]/p \quad (2)$$

In the above equations j is the current density in $10^{-3}$ A/cm$^2$, p is the pressure in mtorr and the remaining constants come from Table II [3].

Table II, Constants for Aston Abnormal-glow Equations for Aluminum as the Cathode Material

| GAS | A | B | E | F$\times 10^{-2}$ |
|---|---|---|---|---|
| Air | 6.5 | 1.33 | 2.55 | 7.27 |
| Argon | 5.4 | 1.07 | 240 | 9.30 |
| Carbon monoxide | 10.0 | 1.33 | 255 | 13.1 |
| Helium | 36.0 | 1.55 | 255 | 31.6 |
| Hydrogen | 26.5 | 1.36 | 144 | 18.1 |
| Nitrogen | 6.8 | 1.26 | 230 | 7.46 |
| Oxygen | 5.7 | 1.55 | 290 | 5.57 |

In the negative glow and the faraday dark space the electric field is close to zero (it may even be negative) and the dominant conduction processes is diffusion. The highly-energetic electrons which are exiting the cathode fall region initially have a relatively low probability of colliding inelastically with gas molecules. After the electrons lose some of their energy the inelastic collision cross section increases, the density of excited atoms and electron-ion pairs increases, and the emitted light intensity peaks (due to photo attachment, ($A + e = A^- + h\nu$) recombination and de-excitation). The electrons continue to lose energy and the emitted light intensity of the discharge decreases through the faraday

dark space. Towards the end of the negative glow region the positive ion space charge density and the electron space charge density approach each other in magnitude.

At the boundary of the positive column the ion space charge density and the electron space charge density become equal and the positive column takes the form of a quasi-neutral, isotropic plasma with a constant electric field. This region is unique in that the length of the region depends on the length of the discharge rather than the pressure, gas type, current density and cathode or anode materials, as do the other parts of the glow discharge. This allows for convenient scaling of systems where the voltage-current properties of the positive column are to be modified. The current scales as the cross section of the discharge and the voltage scales as the positive column length. In the positive column, under steady state conditions, there is a balance between source and loss terms. For example, considering ionization and attachment processes only the rate equation for electron density becomes:

$$dn_e/dt = k_i n_e N_i - k_a n_e N_a = 0 \qquad (3)$$

$$\text{or} \quad k_i/k_a = N_a/N_i \qquad (2)$$

Where $k_i$ and $k_a$ are the ionization and attachment rates respectively. $N_a$, $N_i$ and $n_e$ are the densities of the attacher species, ionizing species and the electrons respectively.

In the anode region the electric potential may be either positive or negative depending on the current density and the value of the electron-anode secondary emission coefficient [4]. At higher current densities the anode voltage must reduce or become positive so as not to repel the incoming electrons. At lower current densities the value of the electron-anode secondary emission coefficient becomes dominant. Electrons are ejected from the anode by secondary emission and travel back toward and into the positive column. This creates a negative space charge which in turn creates a potential drop on the order of magnitude of the ionization energy of the discharge gas.

As the anode is moved towards the cathode, under constant current and pressure conditions, the positive column shrinks and the voltage drops slightly. As the anode enters the faraday dark space the negative glow disappears and the voltage rises. When the cathode-anode distance becomes less than the cathode fall distance the voltage rises at a more rapid rate and the discharge is said to be obstructed.

Effect of a magnetic field on a glow discharge

All regions of a glow discharge are affected by a magnetic field. In this thesis the effects on three regions; the cathode fall region, the negative glow-faraday dark space and the positive column will be separately discussed. In the cathode fall application of

a transverse magnetic field increases the secondary emission coefficient at the cathode boundary [10]. Additionally, the cathode fall potential changes and the cathode fall distance is reduced. It was found experimentally that this effect becomes apparent after a threshold value of magnetic field strength is exceeded [11]. The initial explanation for this effect, given by J. J. Thomson in his 1931 text [11], is related to the helical path taken by the electrons as they traverse the cathode fall region. When the magnetic field intensity is large enough the electrons escape from the cathode fall. However, this model does not take collisional processes into account. In order to take collisions into account, a Monte Carlo simulation method can be used (a method which will be discussed later in this thesis). Figure 3 shows the results of a self consistent Monte Carlo simulation. This figure indicates that a reduction in the cathode fall distance occurs when the magnetic field is increased [12].

In the negative glow-faraday dark space region of the discharge the application of a transverse magnetic field causes the discharge to "bend" in the direction of the field. Additionally, the negative glow distance is reduced and the voltage across the region rises. If the applied magnetic field is parallel to the discharge the negative glow-faraday dark space is extended and the positive column is reduced [11]. Assuming there is enough distance between the cathode and anode so as not to have

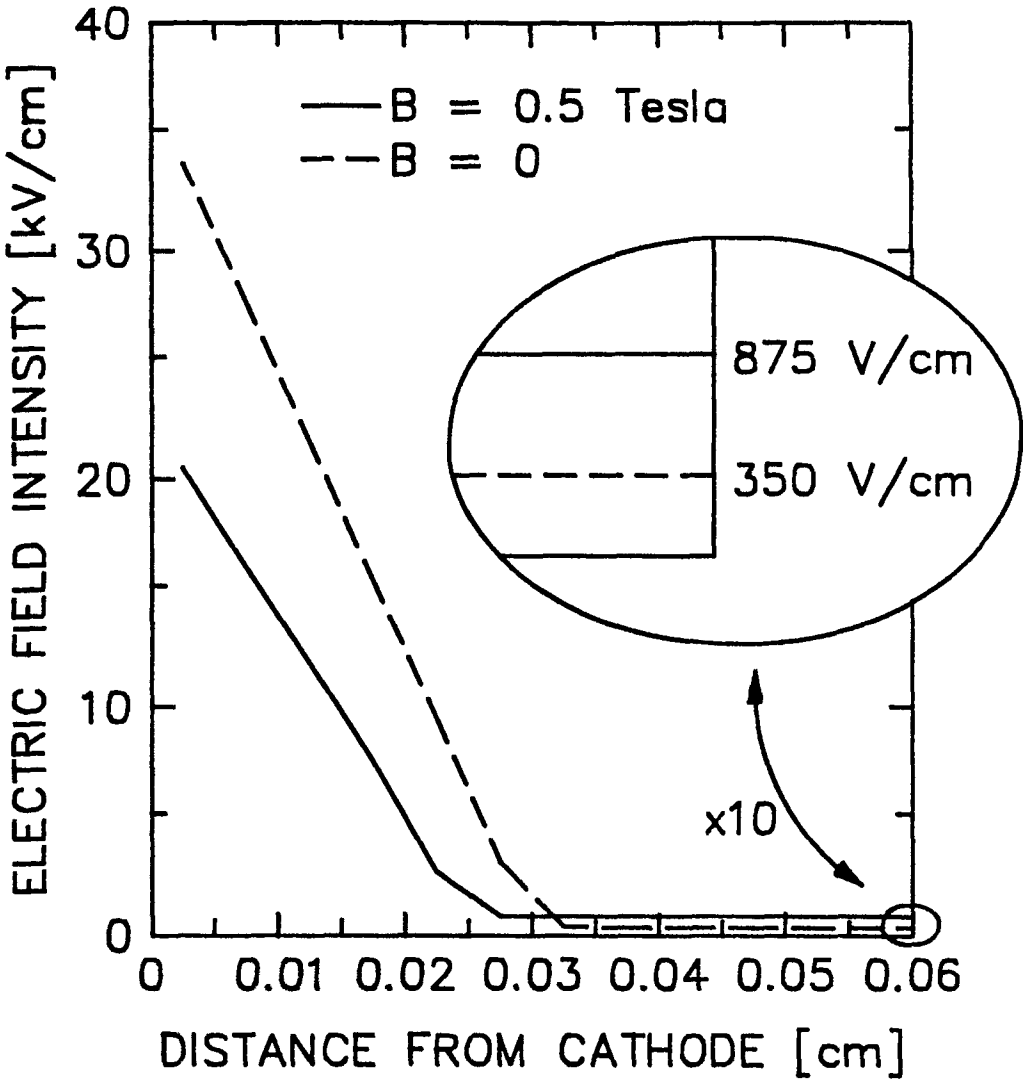


Figure 3. Calculated electric field intensity as a function of distance from the cathode ($J = 1\ A/cm^2$).

an obstructed discharge, there is little or no change in the discharge voltage. If a transverse magnetic field is applied to the positive column, it will be deflected in the direction of the magnetic field. Additionally, the mobility of the electrons is reduced and the positive column voltage rises [13]. A parallel magnetic field will tend to stabilize the positive column and will act as a guide. Using a Monte Carlo technique, it has been determined that application of a transverse magnetic field causes the electron energy distribution in the positive column to be shifted downward. See Figure 4.

Experiments were done as early as 1901 [14] in which the effect of the transverse magnetic fields on the pressure vs cathode fall voltage curve (See Figure 5) was studied. The experiment was performed by applying a local transverse magnetic field to the cathode fall region. It was found that the intersection point of the two curves increases in pressure as both the current density and magnetic field strength increase. Additionally, it was determined that the application of a transverse magnetic field at any other point along the discharge increases the discharge voltage.

Magnetic Control of Glow Discharges

The mechanisms which control the characteristics of a glow discharge with a transverse magnetic field are determined by the gas pressure. For low pressure where the collision frequency is much less than the clyclotron

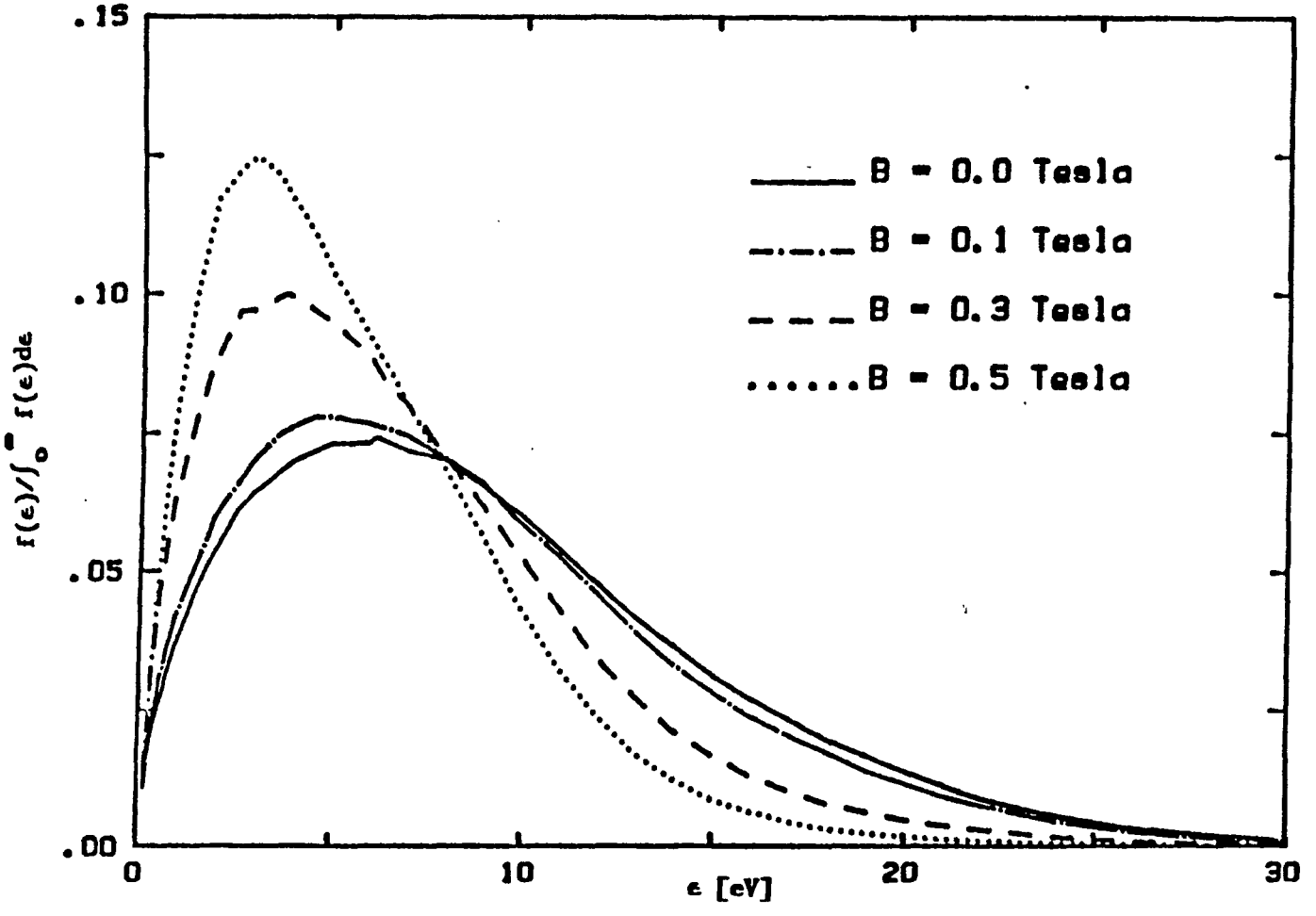


Figure 4. Calculated electron energy distribution in the positive column as a function of applied transverse magnetic field [20]. P = 10 torr, E/N = 120 Td, 20% $SF_6$ - 80% He.

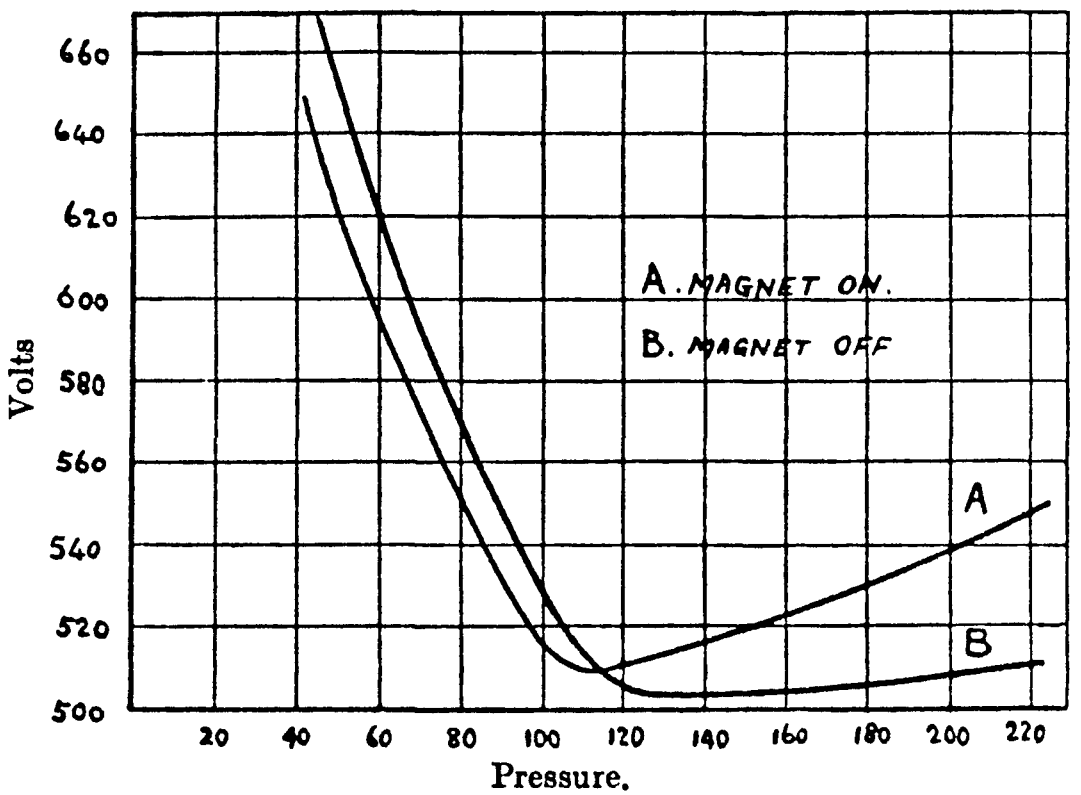


Figure 5. Pressure-voltage characteristics of a glow discharge with a transverse magnetic field applied to the cathode fall region [14].

frequency, the discharge may be described as follows: A primary electron leaves the cathode and follows a modified cycloidal path (see Appendix B). If the separation of the electrodes is greater than the cycloidal orbit height conduction can only occur when the electrons strike gas molecules. Because the pressure and applied magnetic field intensity are such that this event is not probable conduction will not occur until the magnetic field is reduced. This is the first method of controlling a glow discharge using a magnetic field. This phenomenon may be used to control a low pressure closing switch by applying a magnetic field and removing the field to turn the switch on. [15]

The second method of controlling a glow discharge with a magnetic field is to operate the discharge at a slightly higher pressure and control the length of the cathode fall region using a crossed magnetic field. This method has been used by Lutz and Hofmann [16] as a closing and opening switch at current densities up to 5 $A/cm^2$ and voltages of 100 kV. A drawing of this device, known as a gamitron, is shown in Figure 6. The switch is operated on the left side of the critical point of Figure 5. The radioactive $\gamma$ source in the tube center is provided to reduce the statistical time lag which controls the delay between the application of an electric field and conduction, see Figure 7.

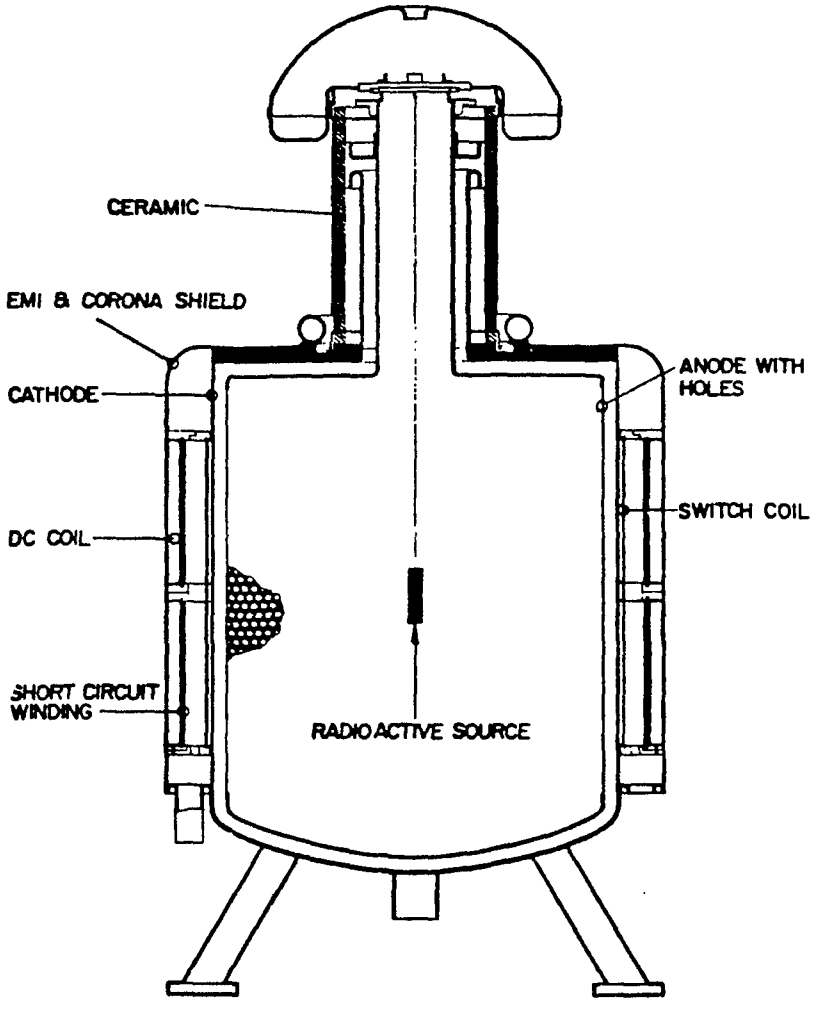


Figure 6. The gamitron, a magnetically controlled cross-field switch [16].

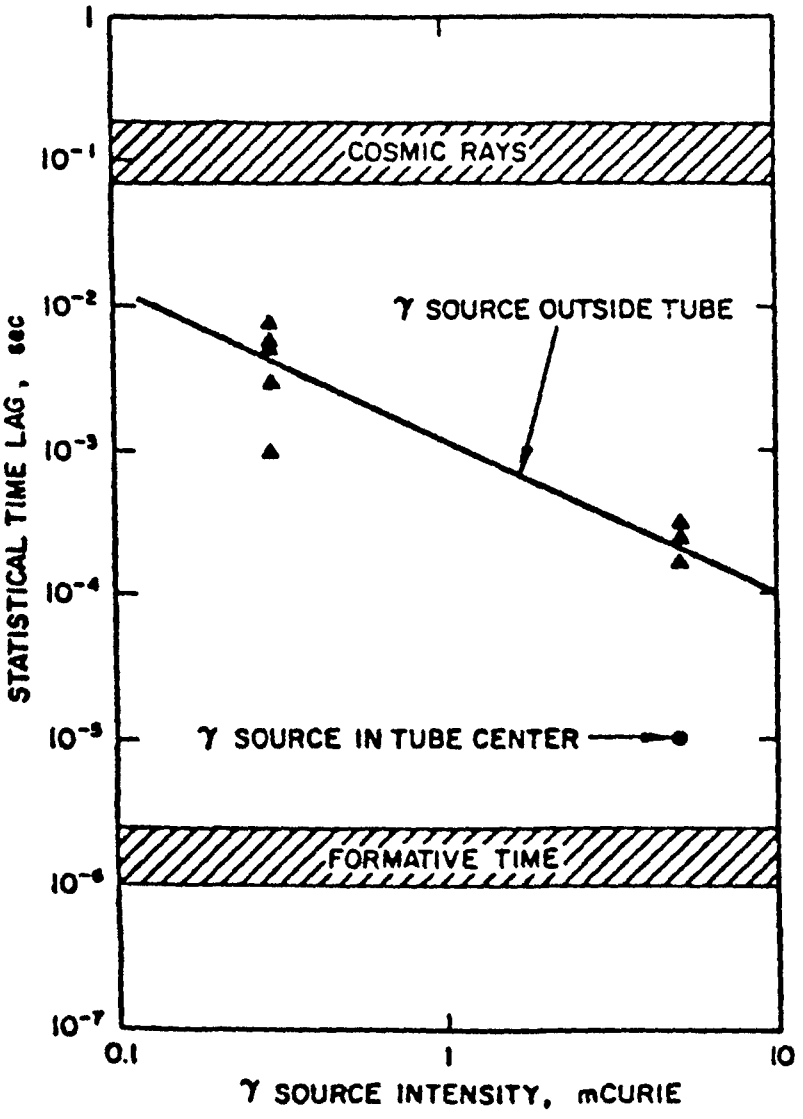


Figure 7. Statistical delay as a function of radiation intensity for the gamitron switch [16].

The switch is operated by obtaining a discharge with an applied magnetic field and removing or counter pulsing the field. Below the critical value of magnetic field intensity, $B_c$ [gauss] = $3.37(V_d)^2/d$ where $V_d$ is the discharge voltage and d is the cathode to anode gap distance in cm, ionization decreases, the cathode fall distance increases to the point of obstruction and the switch voltage rises [16]. The measured rate of rise of the switch was 2 kV/uS with hold-off voltages of over 100 kV and at current levels of 1000 A. At higher currents it was found that there could be localized areas of low magnetic field and high conductivity leading to current channels and subsequent arcing. To correct this the rate of decay of the magnetic field must be on the same order or faster than that of the plasma.

The third method of controlling a glow discharge is to control the voltage-current properties of the positive column. As stated earlier, the voltage of the positive column will increase with the application of a transverse magnetic field. This was demonstrated by Turnquist [13] in 1976. His system was a linear or bifilar tube (see Figure 8) with the cathode fall region outside of the field. The experiment was operated between 0.1 and 0.5 torr with a discharge path about 15 cm long. The stated reason for the increase in discharge voltage was a decrease in the electron mobility $\mu_e$, given by equation (3). According to this equation, in pure He at

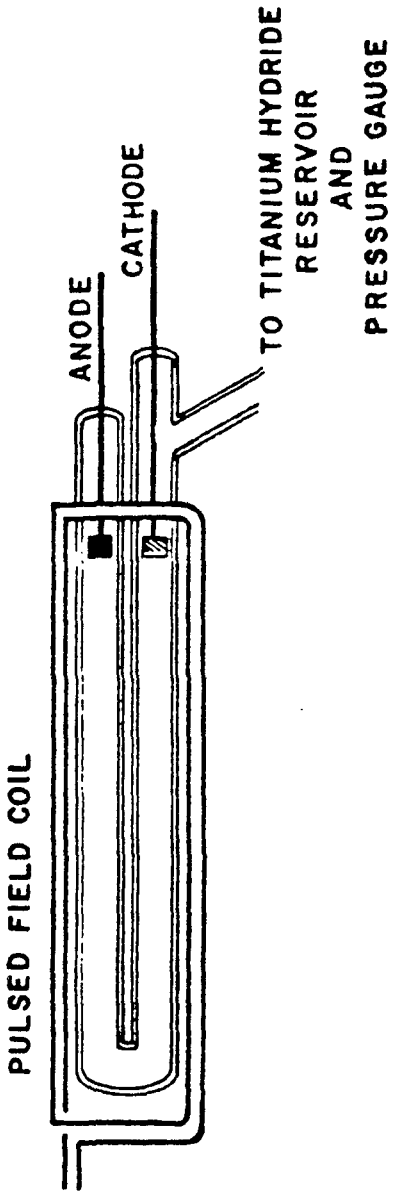


Figure 8. Bifilar discharge tube used by Turnquist [13].

0.5 torr, the mobility may be reduced from 153 $m^2$/V-sec to 0.65 $m^2$/V-sec by applying a 0.1 tesla transverse magnetic field. At 10 torr the mobility would only be changed from 7.6 $m^2$/V-sec to 4.8 $m^2$/V-sec. The major assumption for this approach is that the collision frequency is constant (not a function of $\underline{E}$ and $\underline{B}$).

$$\mu_{ex} = v_x/E = (\nu_c/B\omega_c)/[1 + (\nu_c/\omega_c)^2] \qquad (3)$$

$$\nu_c = 2.3 \times 10^9 \; p[\text{torr}] \quad \text{for He}$$
$$\nu_c = 4.8 \times 10^9 \; p[\text{torr}] \quad \text{for } H_2$$

$$\mu_{ex} = 0.0132p/(B^2 + 1.72\times10^{-4}p^2) \text{ for He} \qquad (4)$$

The assumption that only the mobility is changed when a transverse magnetic field is applied is not correct. Magnetic field controlled gain and loss processes for the electron density play an equal or larger role in the current control process. [17]

When an electron impacts a gas molecule it undergoes either an inelastic collision or there is an elastic collision. In an elastic collision the electron loses only a small portion of its energy. There is, however, a substantial change of its momentum. In an inelastic collision the electron provides energy to the gas molecule or ion. This energy may be used to release an electron as in ionization; or to accept an electron as in attachment or recombination. The physical quantity used when discussing collisional processes is the collision cross section, $\sigma_c$. The collision cross section is

related to the collision frequency $\nu_c$ as shown in equation (7),

$$\nu_c(v) = N_j \; v \; \sigma_c(v) \qquad (7)$$

where $N_j$ is the density of the molecule with which the electron is colliding and v is the electron velocity. Since the collision cross section is a function of the electron velocity the collision frequency is a function of velocity. Collision cross sections for ionization, attachment and elastic collisions for various gases are given in Figures 9, 10 and 11 respectively. Some important collisional processes along with a description of each are given in Table III.

Table III, typical electron-atom (or molecule) interaction processes.

| Process Equation | Description |
|---|---|
| $AB + e^- \rightarrow A^- + B$ | Dissociative-attachment |
| $A + B + e^- \rightarrow A^- + B^*$ | Three body attachment |
| $A + e^- \rightarrow A^- + h\nu$ | Photo-attachment |
| $A + B + e^- \rightarrow A^+ + B + 2e^-$ | Three body ionization |
| $A^- + h\nu \rightarrow A + e^-$ | Photo-detachment |

Figure 12, which gives the result of Monte Carlo calculations, indicates that the collision frequency is not a constant with respect to applied electric or magnetic fields. From the graph, if $\underline{E}$ is held constant, the collision frequency increases with pressure at a rate much slower than linear. Additionally, if p is held

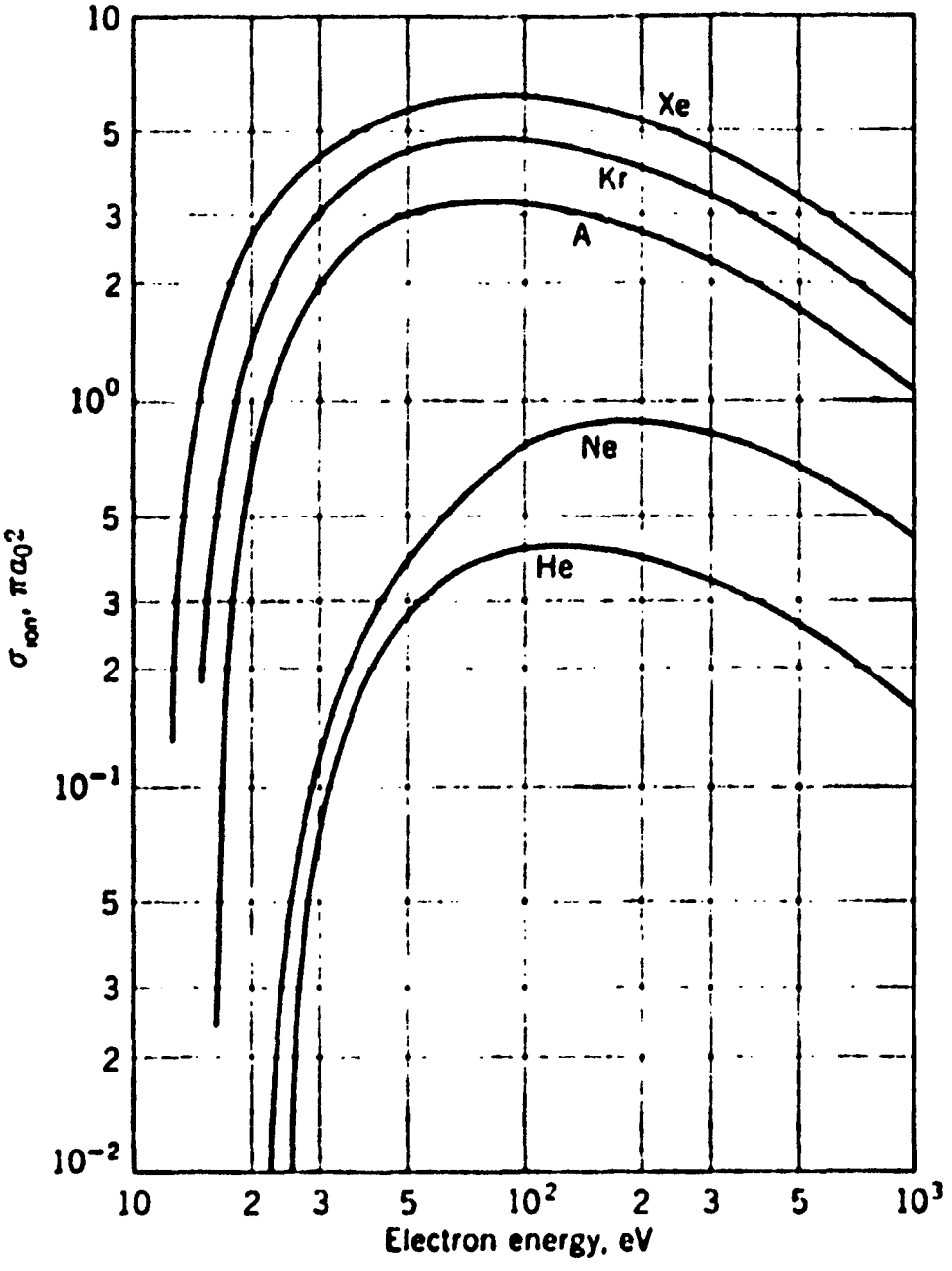


Figure 9. Ionization cross section for various gases [2].

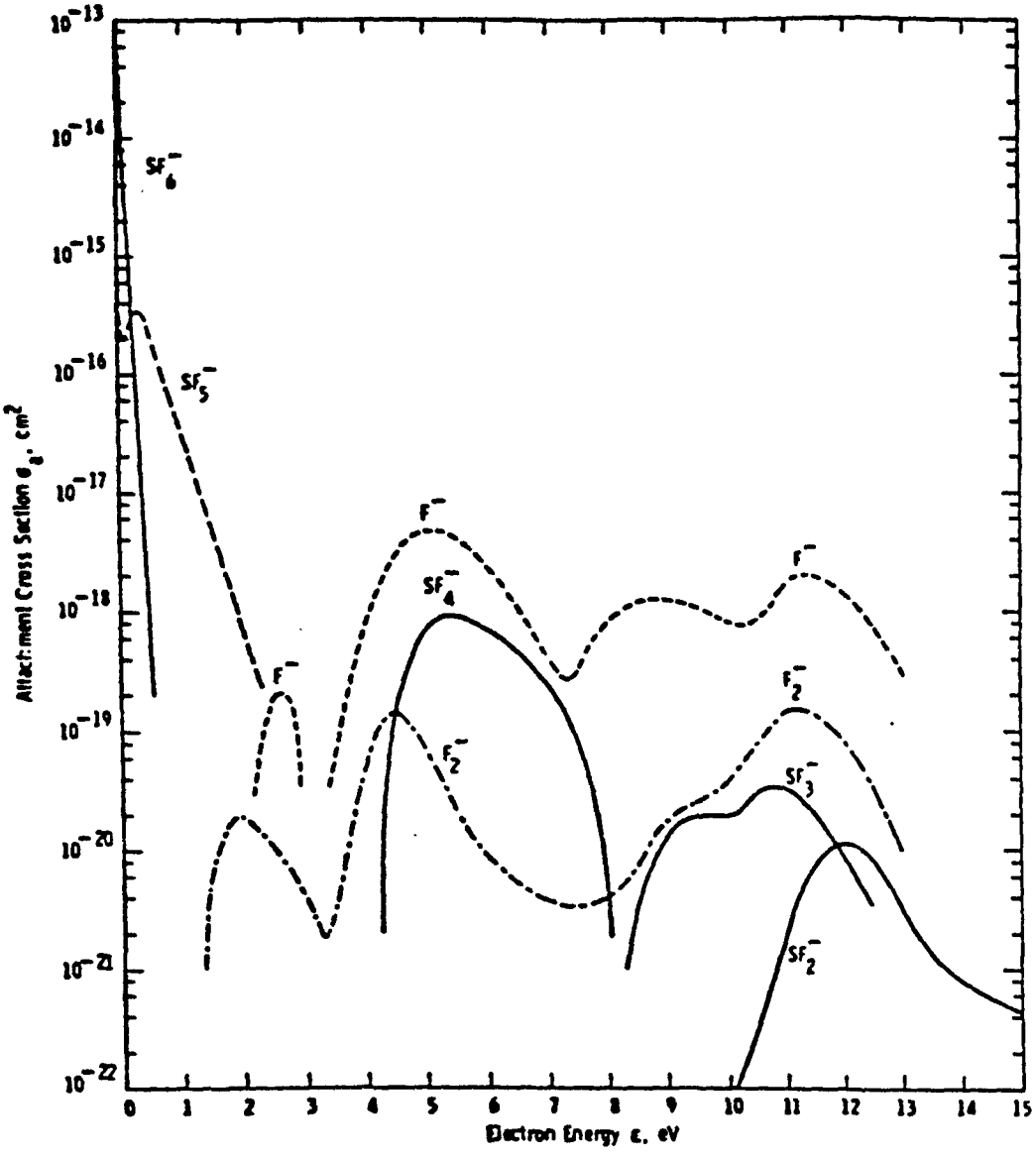


Figure 10. Attachment cross section for $SF_6$ [18].

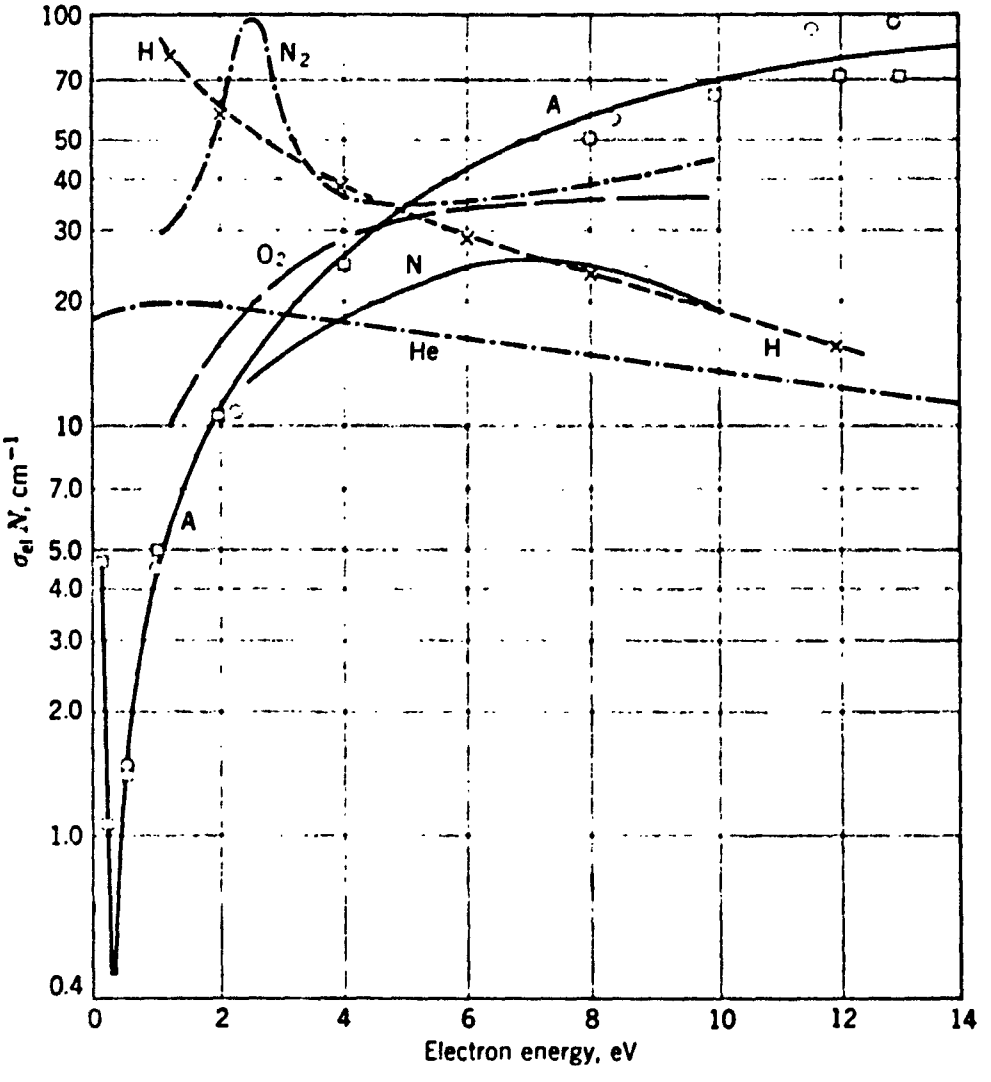


Figure 11. Elastic collision cross section for various gases [2].

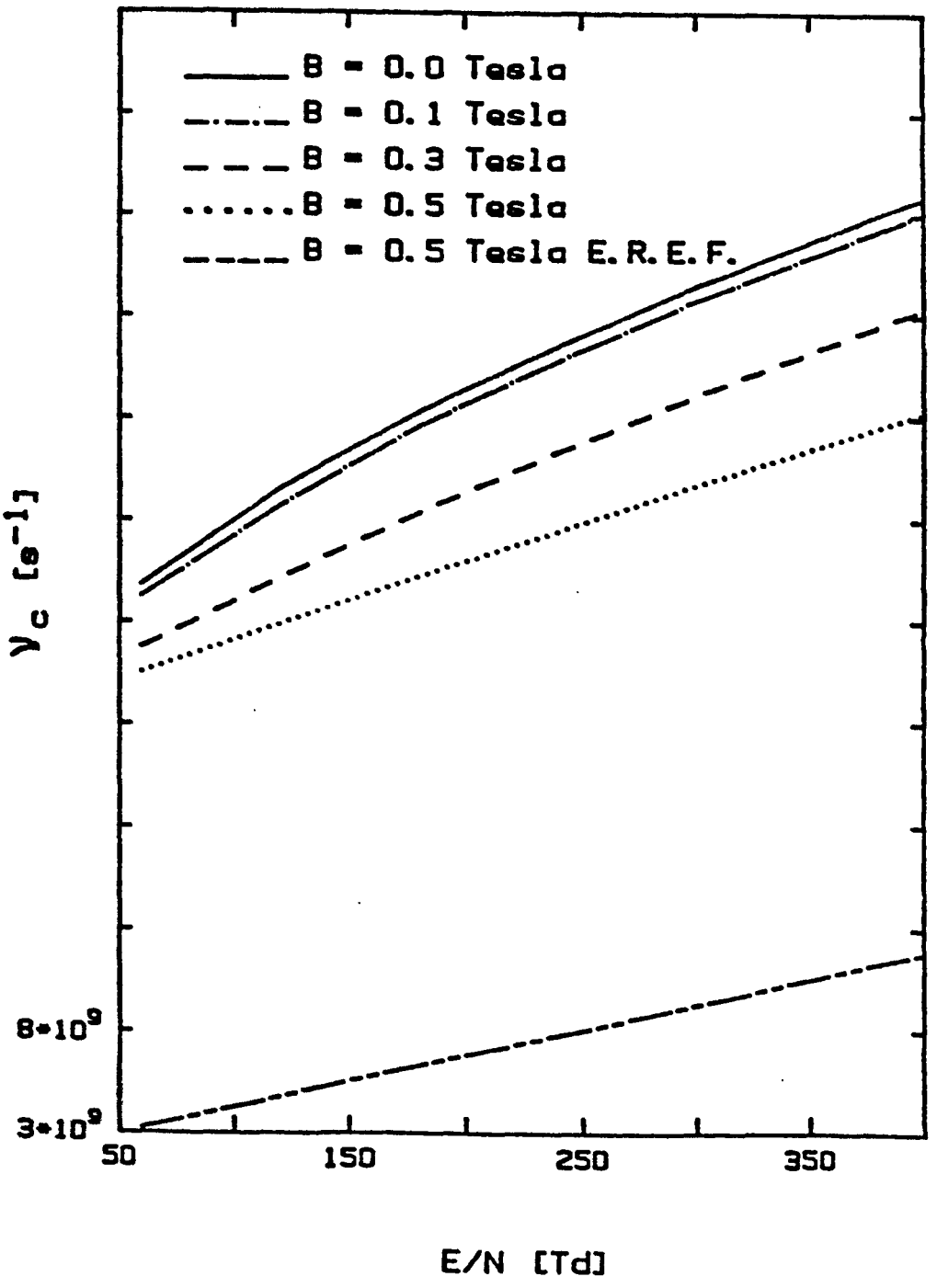


Figure 12. Calculated collision frequency as a function of reduced electric field intensity for various values of magnetic field intensity [20]. p = 10 torr, 20% $SF_6$ - 80% He.

constant, the collision frequency increases with increasing electric field and decreases with increasing magnetic field. Both of these tendencies will enhance the switch operation. If the switch is operated to the left of the critical point in Figure 5, the application of a transverse magnetic field will cause a rise in both the cathode fall voltage and the positive column voltage. Both of these mechanisms will contribute to the desired opening switch action.

## Chapter II
## DISCHARGE MODELING

Several models of glow discharges have been developed. The early models dealt primarily with steady state low current discharges and the conditions at which breakdown occurs. The current levels covered are those at which the electric field in the discharge is uniform between the electrodes. A treatment of this material may be found in several different texts (Thomson [11], VonEngel [5], Cobine [3], Nasser [2]). The basic relationship between the voltage and the current in the discharge is given as

$$J = \frac{J_o[e(\alpha-a)d-a/\alpha])}{[(\alpha-a)/\alpha]-\gamma[e^{(\alpha-a)d}-1]} \qquad (8)$$

where $J_o$ is the primary current due to field emission or photo emission, d is the gap spacing, $\gamma$ is the Townsend secondary emission coefficient, $\alpha$ and a are the ionization and attachment rates respectively.

The voltage current relationship described by equation 8 does not address the steady state conditions found in a glow discharge in the normal and abnormal glow region. Other models which describe the characteristics of various regions of a glow have been developed. This chapter will introduce some of these models.

The Cathode Fall (normal)

As was stated in chapter I, a considerable part of the voltage drop in a glow discharge is across the cathode fall region. This region is characterized by a decreasing electric field which may be approximated as [5]

$$E = E_o(1-x/d_n) \tag{9}$$

where x is the distance measured from the cathode to the anode, $E_o$ is the electric field intensity at the cathode and $d_n$ is the cathode fall distance. Von Engel uses this assumption and the concept of an effective ionization rate to obtain an expression for the normal cathode fall voltage.[5]

$$V_n = (1/\eta)\ \ln(1 + 1/\eta). \tag{10}$$

The effective ionization rate, $\eta$, is the average number of electron-ion pairs per volt produced by an electron in the gas.

As the current density increases and the discharge takes on the characteristics of an abnormal glow, the cathode fall voltage increases and Equation 10 no longer holds. In this region the cathode fall distance, $d_c$, decreases inversely with the average ionization coefficient, $\kappa$. It is weakly dependent on the Townsend secondary emission coefficient, $\gamma$, the cathode fall voltage, $V_c$, the total number of ion pairs, $z_g$, the number of electrons in the swarm, a, and the fast electrons, (1-a). The current density is proportional to $V^{3/2}$ (space charge limited), and a quadratic function of

the average ionization coefficient, $\kappa$. The relationship between the cathode fall voltage and current density and that of the cathode fall distance and voltage was derived [5] to be:

$$j/p^2 \sim V_c^{3/2}/[\ln\{(1/\eta)/(a + (1-a)V_c/z_g)\}^2(\alpha/p)^2 \quad (11)$$

$$pd_c \sim (p/\kappa)\ln[(1/\gamma)/(a + (1-a)V_c/z_g)] \quad (12)$$

where $\kappa/p = f(E/p)$, $a = 1$ for $V_c = V_n$ and decreases as $V_c$ rises, and $z_g$ is the total number of ion pairs per volt in the glow. The numerical values of the constants are given only for He and Cu electrodes.

The Positive Column

Two different models may be used to describe the positive column. These two models are differentiated by the dominant electron loss mechanism which is dependent on the pressure, current and gas processes. At low pressure and low current in gases with a low attachment or recombination rate the diffusion-dominated model is used. At higher pressures, higher current or when gases with high attachment or recombination rates are encountered the attachment/recombination-dominated model is used.

Diffusion-Dominated Model If the following assumptions are made:

1. One step ionization
2. Diffusion losses only
3. Ambipolar diffusion
4. Maxwellian electron distribution
5. Uniform temperature

6. Single species of positive ions
7. No contributions from excited species in the discharge.

It can be shown that the electron temperature in a cylindrical positive column of radius R and number density N is proportional to $N^2R^2$ [21].

Because the electron temperature is assumed to be constant, the longitudinal electric field in the positive column may be determined by balancing the energy electrons gain from the electric field with the that lost due to elastic collisions. The power gained per unit volume from the electric field is

$$P = \underline{J} \cdot \underline{E} = \sigma E^2 \qquad (13)$$

Dividing by the electron density gives the power gained per electron.

$$dP_{gain} = \sigma E^2/n_e \qquad (14)$$

The energy lost per second per electron due to elastic collisions is

$$dP_{lost} = \delta\langle \nu_c \, m_e \, v^2/2\rangle \qquad (15)$$

where $\delta$ is the fractional energy lost at each collision that is approximated by

$$\delta = (2m/M)(1 - \cos\theta) \qquad (16)$$

This leads to

$$(E/N)^2 = 3/2 \, (\delta \, m \, \nu_o^2 \, k \, T_e \,)/e^2 \qquad (17)$$

where $\nu_o = \nu_c / N_o$ and $N_o$ is the number density at one torr. This is to say that E/N is independent of the

electron density, $n_e$, or that it is independent of the current density.

Attachment-Recombination Dominant Model When the dominant processes are attachment and recombination the continuity equation becomes

$$dn_e/dt + \bar{\nabla}\cdot(n_e v_e) = k_i n_e N_i - k_a n_e N_a - k_r n_e^2. \quad (18)$$

In a steady state, homogeneous case the left hand side is zero and the equation reduces to

$$k_i n_e N_i - k_a n_e N_a - k_r n_e^2 = 0. \quad (19)$$

If the discharge is weakly ionized (low current densities) and $k_a N_a >> k_r n_e$ Equation 19 further reduces to

$$k_a/k_i = N_i/N_a. \quad (20)$$

Since the attachment and ionization rates, $k_a$ and $k_i$, are both functions of E/N, E/N may be calculated as the value at which Equation 20 holds true. Because Equation 20 does not contain the electron density, E/N is not a function of the current density.

When the current density increases and $k_r n_e >> k_a N_a$ Equation 20 reduces to

$$k_i N_i = k_r n_e. \quad (21)$$

As the current density (eg. electron density) increases the ionization rate must increase which causes a rise in E/N. When $k_r n_e$ is on the same

order as $k_a N_a$, then the electric field is determined by the condition that

$$k_i N_i - k_a N_a - k_r n_e^2 = 0. \quad (22)$$

Effects of a Transverse Magnetic Field

The effect of a transverse magnetic field on the motion of a group of electrons is described using Langevin's equation:

$$m_e d\underline{v}_e/dt = -e(\underline{E} + \underline{v}_e \times \underline{B}) - m\nu_c \underline{v}_e \quad (23)$$

where $\nu_c$ is the collision frequency at the effective electric field value. If $\underline{E}$ is in the positive-x direction and $\underline{B}$ is in the positive-z direction the solution of this equation is given as Equations (24) and (25).

$$v_x = Ee/m_e \, \nu_c \, [1/(1 + \omega_c^2 / \nu_c^2)] \quad (24)$$

$$v_y = Ee/m_e [\omega_c / (1 + \omega_c^2 / \nu_c^2)] \quad (25)$$

The direction taken by electrons is in the $\theta$ direction where

$$\tan \theta = v_y / v_x = eB/m\nu_c. \quad (26)$$

This means that the effective electric field that the electrons see is

$$E_e = E \cos \theta \quad (27)$$

or

$$(E/N)_e = E/N \, [1 + (e/m\nu_o)^2 (B/N)^2]^{-1/2}, \quad (28)$$

where

$$\nu_o = \nu_c / N_o, \quad (29)$$

and $N_o$ is the number density at one torr. Equation 28 may also be written as

$$E/N = (E/N)_e \left[1 + (e/m\nu_o)^2(B/N)^2\right]^{1/2}. \qquad (30)$$

According to Equation (30) the application of a transverse magnetic field increases the working electric field of the positive column. For large B/N, E/N becomes proportional to B/N.

The major assumption is that the collision frequency is not a function of the electron energy or applied electric field. Figure 12 shows that the collision frequency, as determined by Monte Carlo calculations, is actually a function of the applied electric field and the transverse magnetic field [20]. For this reason a thorough discharge analysis requires numerical methods.

Discharge Simulation Techniques

Several methods of simulating a glow discharge have been used in recent years [19,22]. These methods include using the Boltzmann equation, use of continuum models and monte carlo techniques. All of these methods involve numerical simulation.

In the Boltzmann method [23] the electrons are represented by a time-dependent distribution function in phase space, $F(\underline{r},\underline{v},t)$. A time dependent continuity equation of the distribution functions is written in terms of particle flow across boundaries of a unit cube in phase space, $d\underline{r}^3d\underline{v}^3$. This equation is known as Boltzmann's equation. It is expanded in terms of Legendre functions in the angular coordinates of velocity which is truncated

at the desired accuracy. Approximations are made for the appropriate collision cross sections. The Boltzmann equation is then reduced to a system of coupled linear differential equations which are solved numerically for the desired transport coefficients and the electron energy distributions. This method is appropriate for all regions of a glow discharge [22].

The Monte Carlo method is a computer experiment. In this method an electron is followed as it moves through the gas. The type of collision along with the electron energy and momentum after each collision are sampled. The type of collision which occurs at each time interval is determined using a random number. If it is an elastic collision, the scattering angle is generated using a new random number. The direction of the particle velocity is adjusted and the electron is accelerated by the fields until the next collision. If the collision is inelastic, a new random number is generated to determine what type of inelastic collision occurs and said collision type is recorded. If the electron has not recombined or attached in this process, then the process is continued. If the electron has recombined or attached, a new electron is introduced and the process is continued. A large number of collisions, typically $10^6$, are followed and the ionization rates, attachment rates and electron energy are recorded.

Monte carlo calculations were done for a 20% $SF_6$ - 80% He mixture for various values of magnetic and electric field in a steady state homogeneous gas (positive column) by Cooper [20]. Figure 3 is the resulting electron energy distributions for various magnetic field intensities [20]. Figures 13 and 14 are the attachment rate and ionization rate versus reduced electric field strength for various magnetic field intensities, respectively. Assuming that the gas system is attachment dominated the condition that

$$k_a/k_i = N_i/N_a \tag{31}$$

holds and the reduced electric field as a function of magnetic field intensity may be determined from Figures 13 and 14. This curve, given as Figure 15, illustrates the effect of a crossed magnetic field on the equilibrium electric field in the positive column.

To explain the increase in reduced electric field strength due to a transverse magnetic field consider Figure 16. When a magnetic field is applied to the discharge, the electron energy distribution shifts downward. This shift occurs because the higher energy electrons have a larger velocity, some of which is transverse to the magnetic field. They thus travel a longer path ($r_L = v_\perp/\omega_c$) and subsequently have a larger probability of undergoing an inelastic collision. When this shift of the electron energy distribution takes place the probability of attachment increases while the

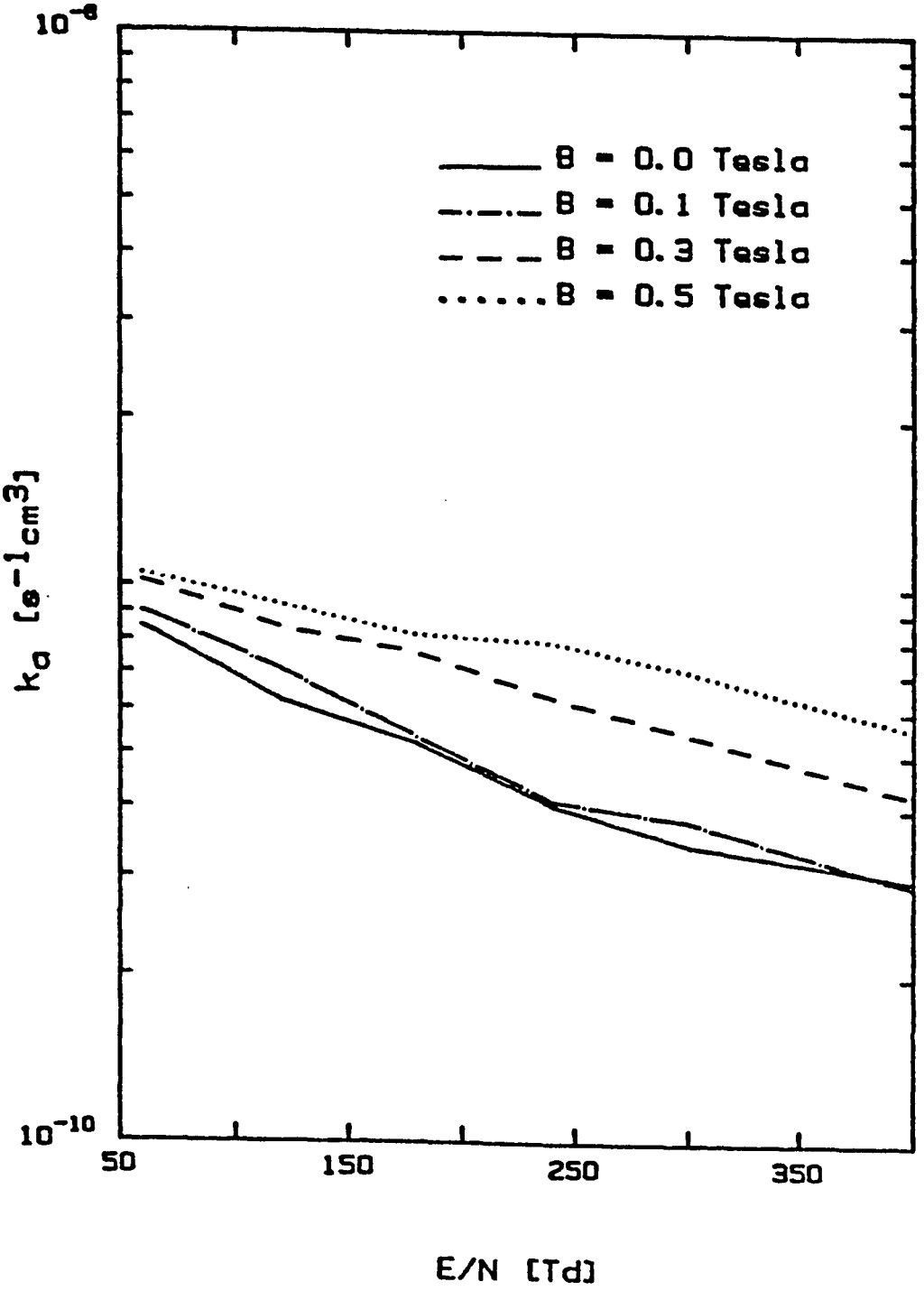


Figure 13. Calculated attachment rate as a function of reduced electric field intensity for various values of transverse magnetic field intensity [20]. P = 10 torr, 20% $SF_6$ - 80% He.

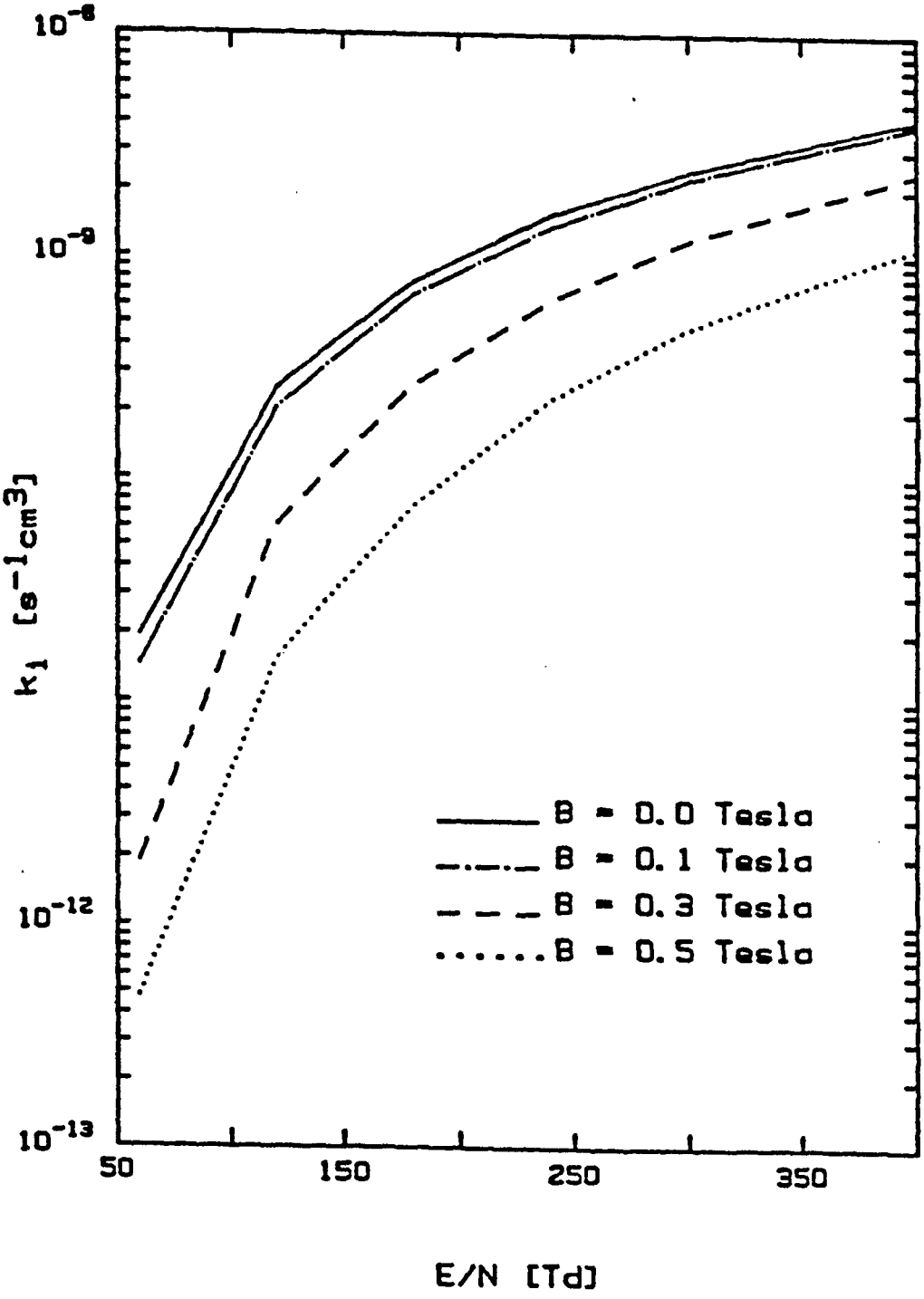


Figure 14. Calculated ionization rate as a function of reduced electric field intensity for various values of transverse magnetic field intensity [20]. P = 10 torr, 20% $SF_6$ - 80% He.

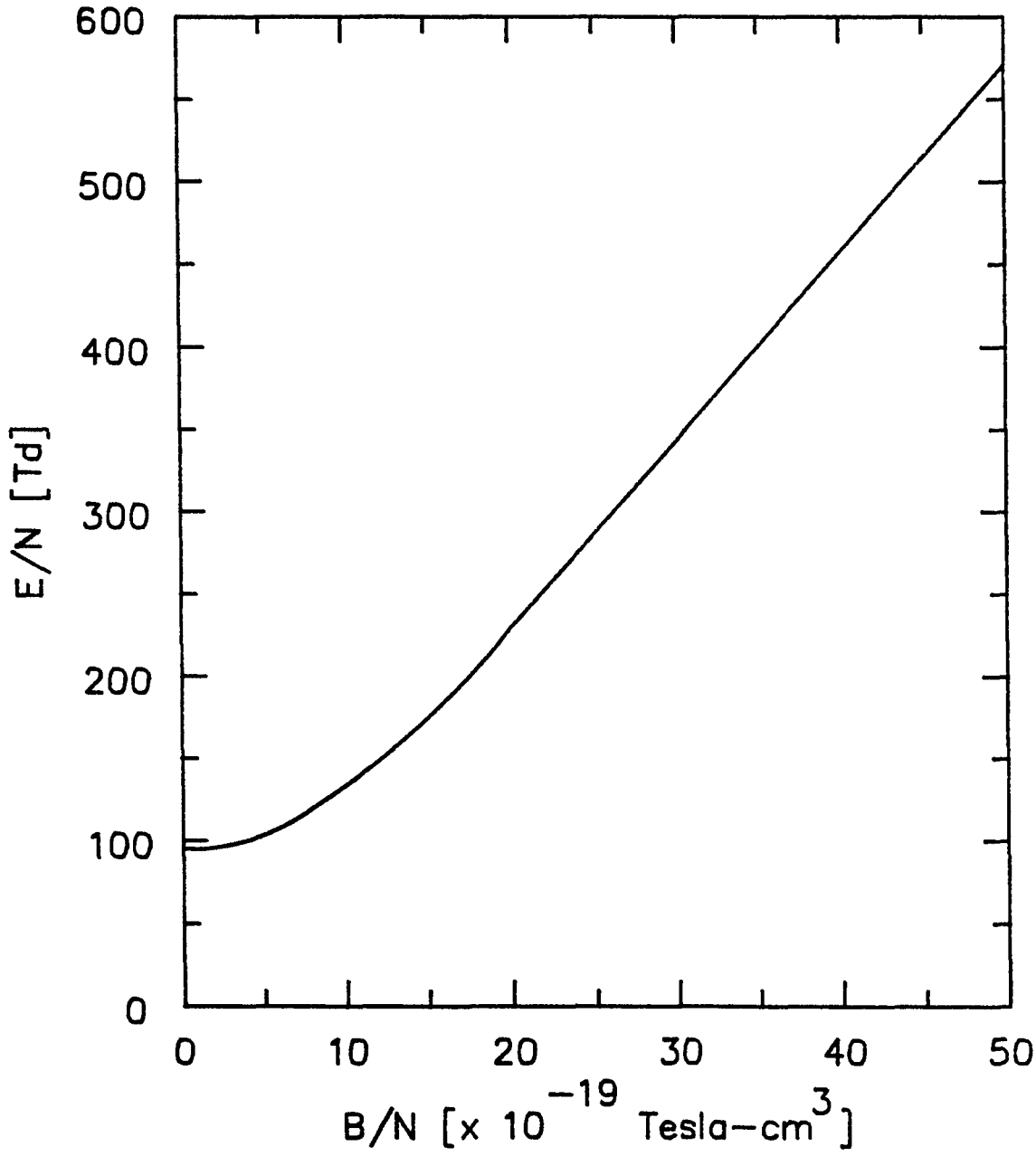


Figure 15. Calculated reduced electric field intensity as a function of reduced magnetic field intensity [20]. P = 10 torr, 20% $SF_6$ - 80% He.

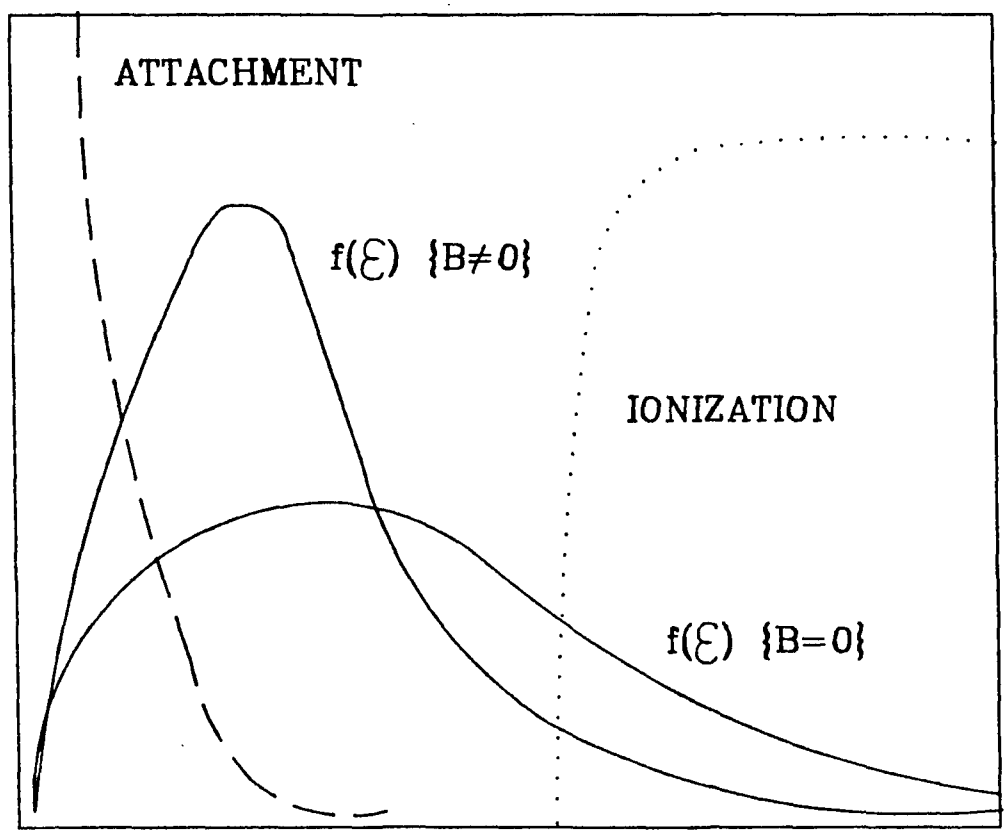


Figure 16. An illustration of the concept of magnetic field control of diffuse discharges.

probability of ionization decreases. This effectively reduces the number density of the electrons and helps to extinguish the discharge [24].

# CHAPTER III
# EXPERIMENTAL SETUP

The experimental setup consists of a co-axial discharge chamber surrounded by a solenoidally shaped coil. This allows the application of a "quasi-dc" axial magnetic field, with peak values of 1.2 Tesla, to a radial glow discharge, of current densities up to 2 $A/cm^2$. The brass center electrode is the cathode. It has a 3.18 cm diameter and a surface area of 100 $cm^2$. The anode consists of a set of twelve 0.32 cm diameter stainless steel rods which are arranged to form a cylinder around the cathode. The cathode to anode gap spacing is 2.06 cm at the minimum point. The quasi-dc magnetic field is obtained by setting the decay time constant of the magnetic field circuit to a value much greater than the pulse length of the electric field circuit. The system may be broken down into three basic blocks as shown in Figure 17. These are the magnetic field circuit, the trigger circuit and the discharge circuit.

## Magnetic Field Circuit

The magnetic circuit is a series RLC circuit consisting of a 45 microfarad capacitor bank, a 970 microhenry inductor, a spark gap switch and a series damping resistor whose value is varied depending on the desired peak current. The series damping resistor is the parallel

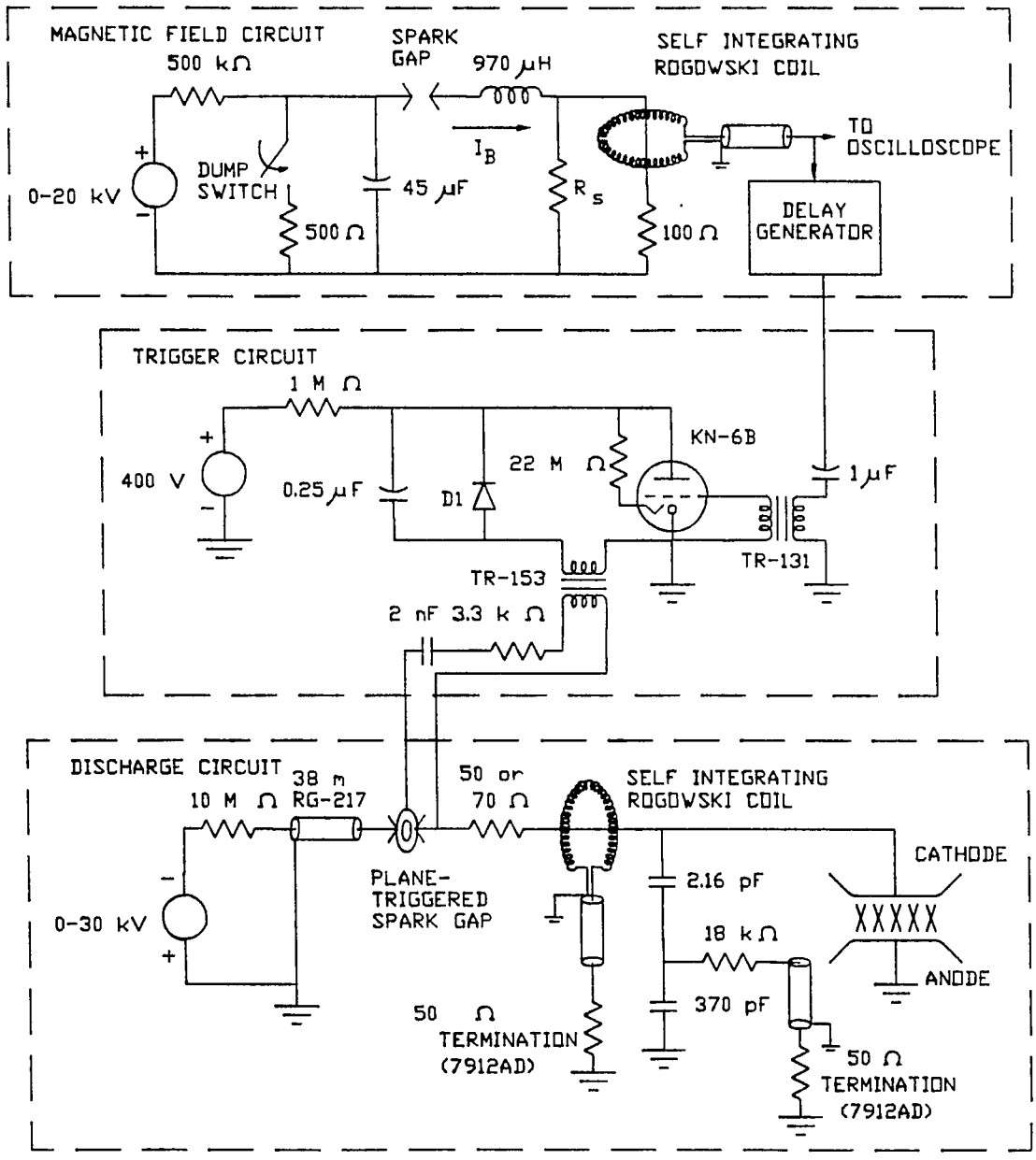


Figure 17. Schematic diagram of the experimental setup.

combination of the 100 Ω resistor and $R_S$. The 100 Ω resistor is a ceramic composite resistor and $R_S$, when it is used, is a low inductance 8.2 Ω or 5.4 Ω wire resistor. An additional requirement on the selection of the damping resistor is that the quality factor, Q, of the circuit remain less than 0.9 to avoid an excessive voltage reversal on the capacitor bank. As discussed in Appendix A, the value of the magnetic field intensity along the axis of the coil varies from 5.4 gauss/amp to 4.1 gauss/amp; for convenience a value of 5.4 gauss/amp is used. With peak currents of 2.2 kA, magnetic fields in excess of 1.2 Tesla were obtained. The current is monitored using a commercially available Rogowski type current monitor. The magnetic field strength is varied using three methods. Either the magnetic field voltage is adjusted by adjusting the p·d value of the switch, the damping resistor ($R_d$) is changed or the delay on the trigger circuit is varied.

Trigger Circuit

System timing is accomplished by sampling the magnetic field current and triggering the electric field circuit after the desired delay. The delay is generated using a commercial delay generator whose output drives the input of the trigger circuit. The front end of the trigger circuit consists of a 0.25 μ capacitor in series with the primary winding of a 51:1 pulse transformer (TR-153) that is charged by the 0-400 volt DC power supply. When the grid of the krytron is pulsed, by the output of the 40:1

transformer (TR-131), the capacitor discharges and current flows through the krytron and hence the pulse transformer. The output of the pulse transformer is applied to the trigger plane of the spark gap in the discharge circuit. The limiting risetime of the trigger circuit is that of the 51:1 pulse transformer which has a risetime of 500 ns [25]. The 3.3 kΩ resistor and the 2 nanofarad capacitor are in the circuit to isolate the trigger circuit from the electric field pulse forming network and to isolate the transformer from the 0-30 kV charging voltage respectively.

Discharge Circuit

The discharge circuit consists of a 0-30 kV power supply in series with a 10 MΩ charging resistor which charges a 38 meter section of RG-217 cable (200 ns). The cable is switched with a plane triggered coaxial spark gap whose trigger plane is driven by the trigger circuit. There is a shielded 70 Ω resistor in series with the coaxial discharge chamber. The shield assembly was added to the system to reduce stray fields and to reduce the inductance. The automatic dump-switch, which closes when power is removed from the high-voltage power supply, is provided as an auxiliary discharge path for the capacitor bank.

The discharge chamber consists of a 10.2 by 3.18 cm diameter brass cathode surrounded by 12 - 14 cm long and 3.2 mm diameter stainless steel anode rods. These rods are separated by a nylon bushing and the entire assembly is

placed in a 90 mm diameter quartz cylinder that is sealed at both ends. This geometry provides a 100 $cm^2$ cathode surface and a discharge region 2.06 cm in length. Additionally, this geometry provides a specific geometry of the cathode surface which is covered by the cathode glow. See figure 18 for a cross-sectional view of the discharge chamber. Typical pressures used in the operation of the system varied from less than 0.1 torr to a maximum of 20 torr. The gases are mixed in a 0.5 l vessel at pressures up to 30 pounds per square inch absolute and then leaked into the chamber as desired. A vacuum was maintained on the chamber by a rotary vacuum pump connected at the opposite end of the chamber from the fill line and vacuum gauge.

Diagnostic System

Both the circuit current and the discharge voltage characteristics were recorded using transient digitizers, and the value of the magnetic field current was sampled using a storage oscilloscope. The voltage was monitored by a capacitive voltage divider in series with a resistive voltage divider. This device has a fast risetime which is limited only by the self inductance of the the two carbon resistors. Ignoring this inductance, the step response of this specific divider network is described by the following equation:

$$V(t)=V_oA\ e^{(-t/\tau)} \qquad (32)$$

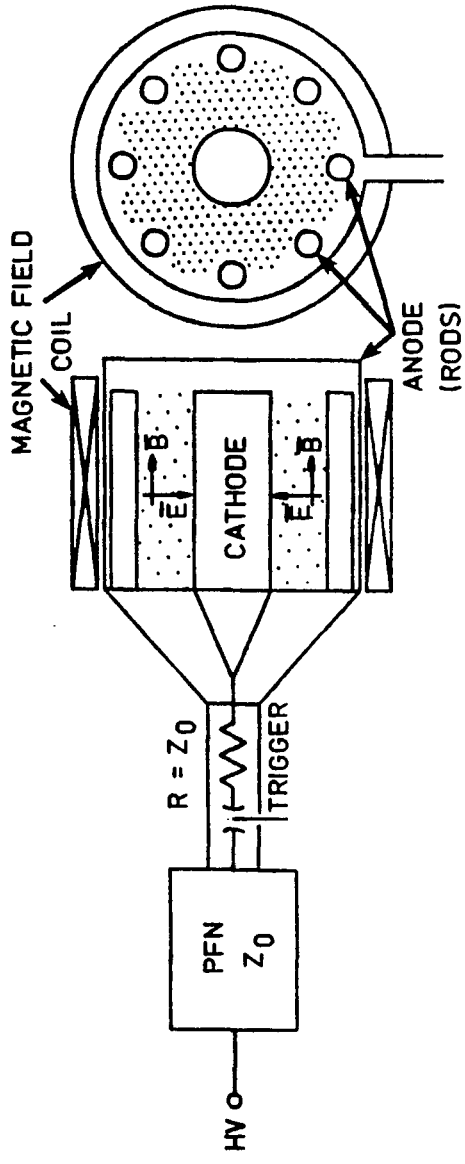


Figure 18. Cross sectional view of the discharge chamber.

with A = 1/61800 and $\tau = 6.6 \times 10^{-6}$ s. A complete description of the derivation of this equation is included in Appendix A of this thesis. As one can see, the above transfer function varies as $e^{(-t/\tau)}$. The factor $e^{(-t/\tau)}$, known as droop, is a measure of merit for the device. For pulses up to 60 ns long this device provides an output which is within one percent of the correct value. For pulses 200 ns long, the length of those generated by the cable discharge, the device provides an output which is within three percent of the correct value. For values far above 200 ns, the device may be used if the waveform data is convoluted in the time domain with the inverse of the transfer function given by

$$X_n = (\tau/\Delta t) \left( \sum_{i=1}^{n} X_i \right) + X_n \qquad (33)$$

where $\Delta t$ is the time between samples, and $X_n$ and $X_i$ are the $n^{th}$ and $i^{th}$ values of the data file with respect to zero. The current was measured with a commercial Rogowski type current monitor which has a 10 nanosecond rise time and droop of 0.008 percent per microsecond. The output of the current monitor is one volt per ampere.

Figure 19 is a plot of the voltage and current waveforms for a 20% $SF_6$ / 80% He mixture with an applied magnetic field of 0.75 Tesla. The ramp in the voltage from 0 to approximately 200 ns, which is never seen under self

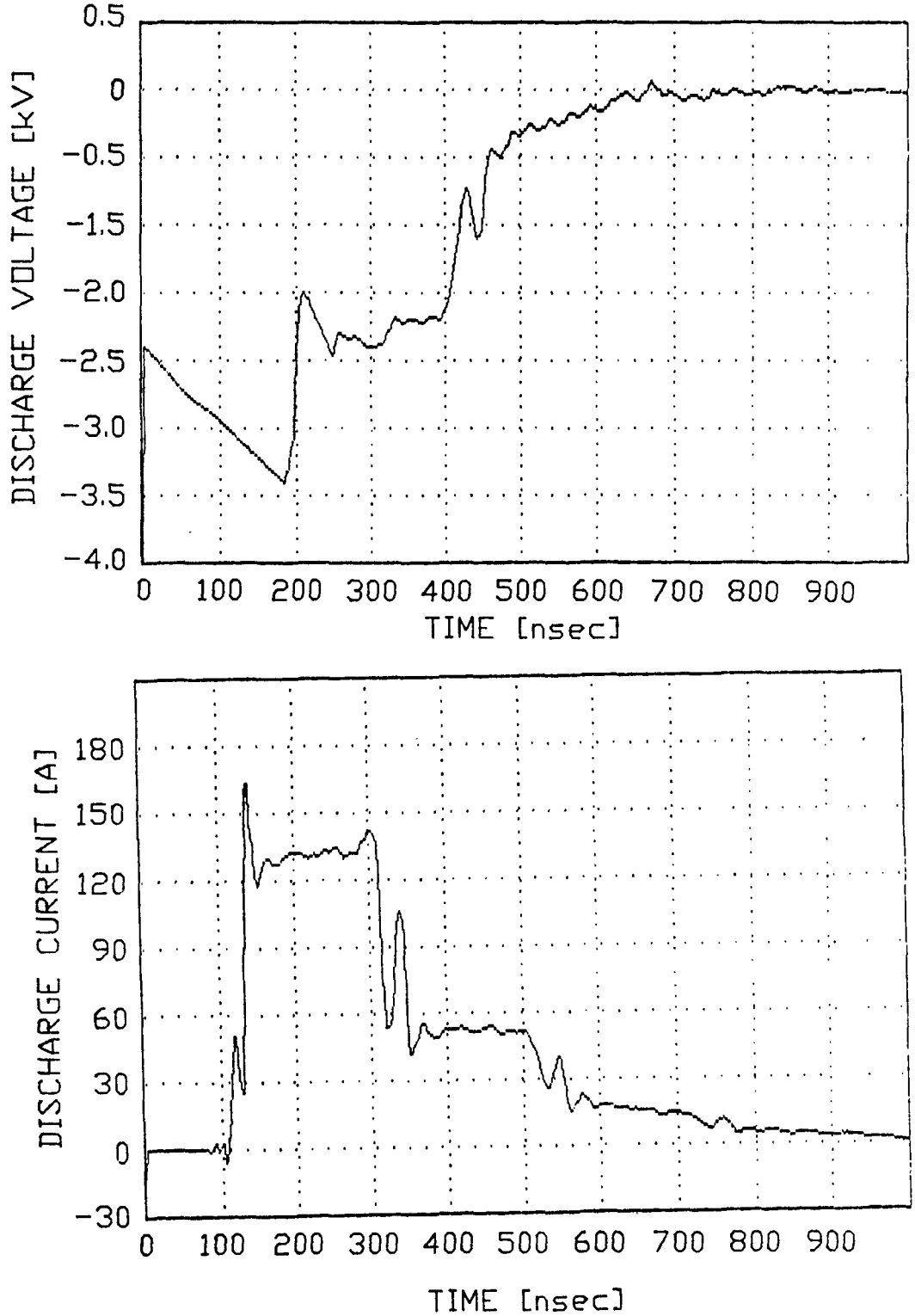


Figure 19. Typical discharge voltage and current waveforms (signals shifted in time due to triggering).

breakdown conditions, is probably due to the stray capacitance between the primary and the secondary windings of the 51:1 pulse transformer in the trigger circuit. At 200 ns the triggered spark gap breaks down, and after an inductive overshoot, the voltage across the discharge decreases to approximately 1900 V and the current rises to approximately 67 A. At 400 ns the first pulse of the transmission line ends. The discharge transitions to an arc. When this occurs, the voltage across the chamber reduces to approximately zero while the current rises slightly but remains approximately 25 A. While this is a typical waveform, not all shots taken broke down on the reflected pulse and in many cases several reflections were seen in the voltage waveform.

# CHAPTER IV
# EXPERIMENTAL RESULTS

## General Discussion

Figure 20a contains the voltage waveforms of four consecutive data points taken under the same conditions plotted on the same graph. The jitter in the original waveforms was corrected by aligning three of the waveforms with the first using an interactive graphics program. The difference in the first 350 ns of the lower three waveforms is due to the statistical delay of the electrical circuit spark gap. On the forth waveform the trigger level was set such that the trace started when the spark gap broke down. After this initial difference, the statistical spread of the amplitude of the data is approximately 10 percent. Figure 20b, and 20c are plots of the average value of each data point in the four waveforms and a plot of one of the waveforms respectively.

There is an additional shot-to-shot error in the voltage signals due to the exponential decay of the capacitive-resistive voltage divider output. This error comes about because of the statistical delay of the discharge breakdown. The longer a DC voltage is applied to the voltage divider the smaller the recorded voltage becomes. This effect is explained in Appendix A.

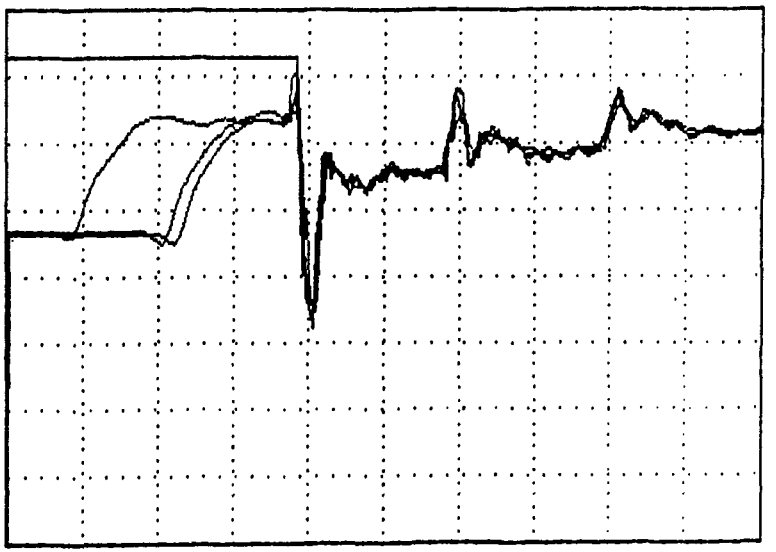

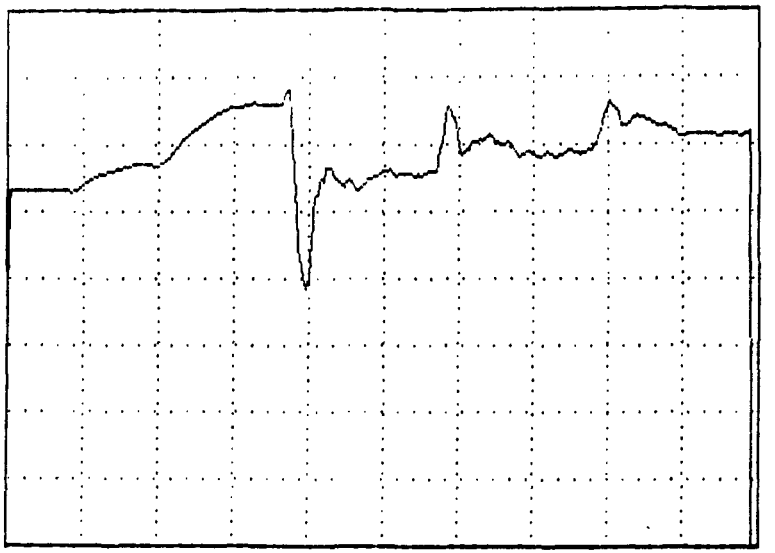

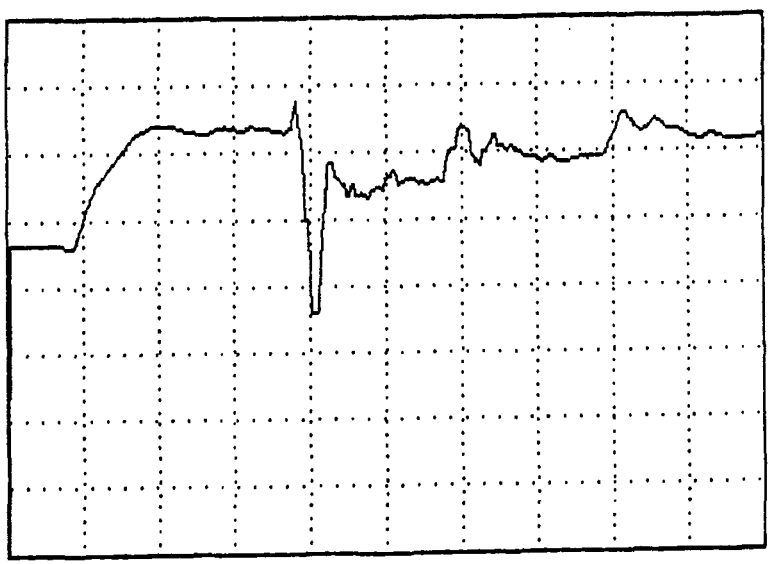

Figure 20. Typical voltage waveforms top left - four consecutive shots, top right - the average of the four shots, bottom left - one of the four shots. Vertical scale is 618 V/div. Horizontal scale is 200 nsec/div.

Figure 21 shows a corrected voltage waveform and the original waveform. As the statistical delay becomes greater the error becomes greater because of the leakage current in the series capacitive-resistive voltage divider. This effect always lowers the indicated voltage. The maximum error due to droop is approximately 15 percent. Compensation is made for droop when the waveforms are evaluated.

The current in the circuit is mainly a function of the applied voltage and the series resistor. Its value does not vary by more than 5 percent from shot to shot for a specific value of applied voltage when the switch in the electrical circuit is externally triggered. However, when the switch in the electrical circuit is in the self breakdown mode the voltage at which the spark gap breaks down varies causing the current to vary from shot to shot. The triggered mode is used for the majority of the work in this thesis. Figure 22a is of an overlay of the current waveforms for the same four shots used in Figure 20. Figures 22b and 22c are also an averaged waveform and original waveform respectively.

It is not uncommon for the discharge to undergo a transition from a glow discharge, with a typical voltage of two kilovolts, to a low voltage arc. The actual value of the discharge voltage could not be measured (because of the relatively low sensitivity of the voltage divider). It was assumed to be on the order of ten volts [1,2].

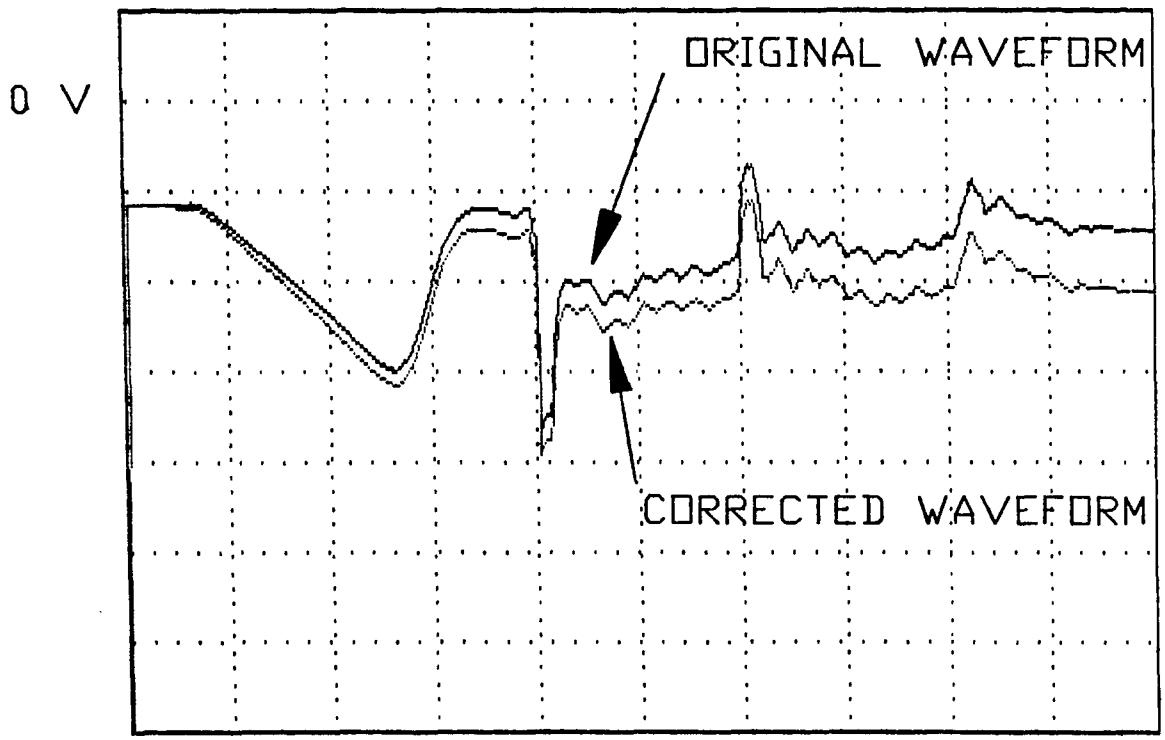


Figure 21. Original (upper) and corrected (lower) voltage waveforms. Vertical scale is 618 V/div. Horizontal scale is 200 nsec/div.

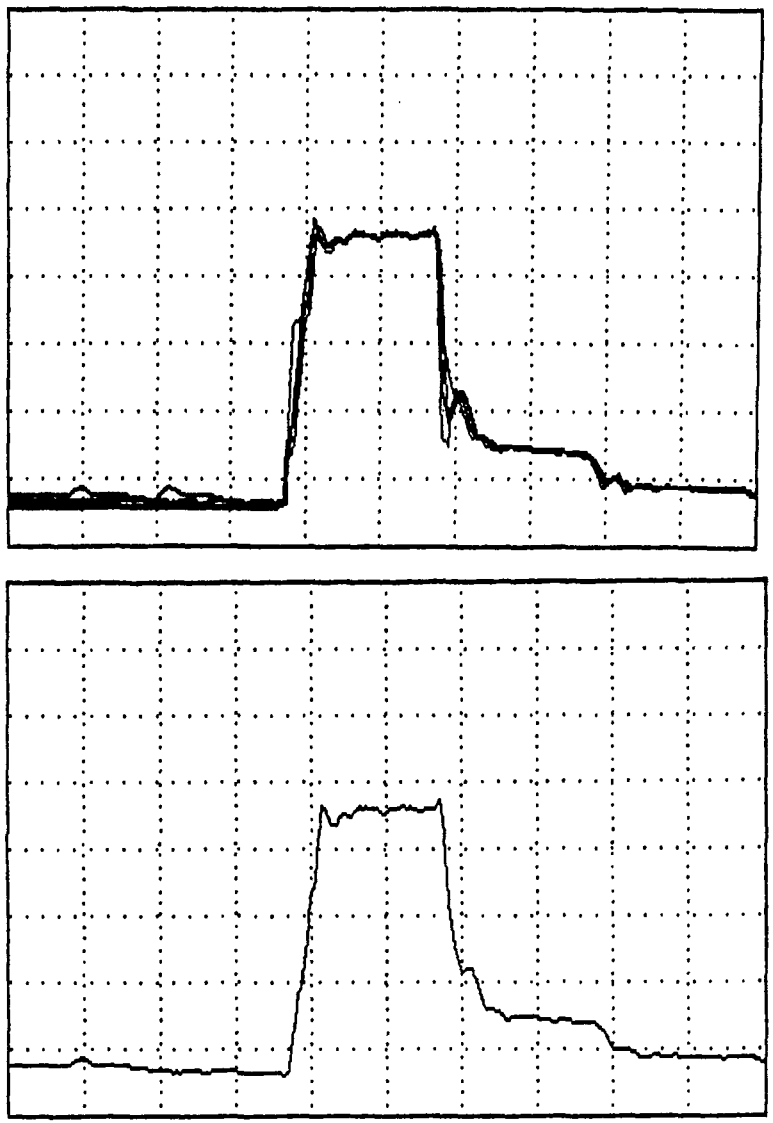

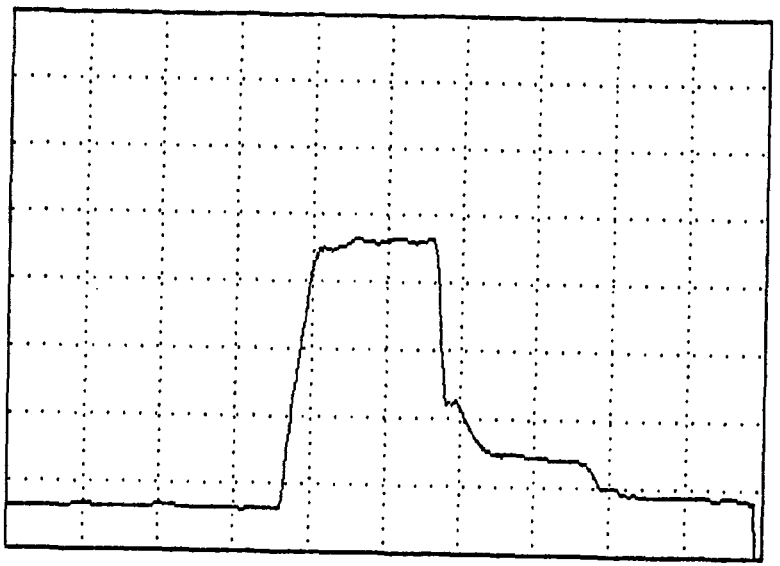

Figure 22. Typical current waveforms top left - four consecutive shots, top right - the average of the four shots, bottom left - one of the four shots. Vertical scale is 15 A/div. Horizontal scale is 200 nsec/div.

When arcs did occur, the value of the discharge voltage prior to the transition was recorded only if the discharge was stable for times longer than 70 ns. This occurs with more regularity and with less of a delay (stable for a shorter amount of time) as the current density or transverse magnetic field intensity is increased. This glow to arc transition limited the measurements to the range of $B < 0.65$ Tesla and the current density $J < 1.5$ A/cm$^2$, where J equals the discharge current divided by the cathode surface area (100 cm$^2$). When higher magnetic fields are applied the discharge voltage is reduced as the current density is increased. This process does not necessarily lead to a glow to arc transition (see Figure 23).

Measurements in He-$SF_6$ at Constant Pressure

Figure 24 gives the measured quasi steady-state voltage current characteristics for the discharge with applied transverse magnetic field. These measurements were made using the experimental setup described in Chapter III with a 20% $SF_6$ - 80% He gas mixture at a pressure of eight torr. The measurements were made by recording both the discharge current and voltage waveforms using two transient digitizers for several values of applied voltage at specific values of magnetic field intensity. Several data points were taken for each value of applied voltage. They were compared graphically and a typical pair of waveforms was selected.

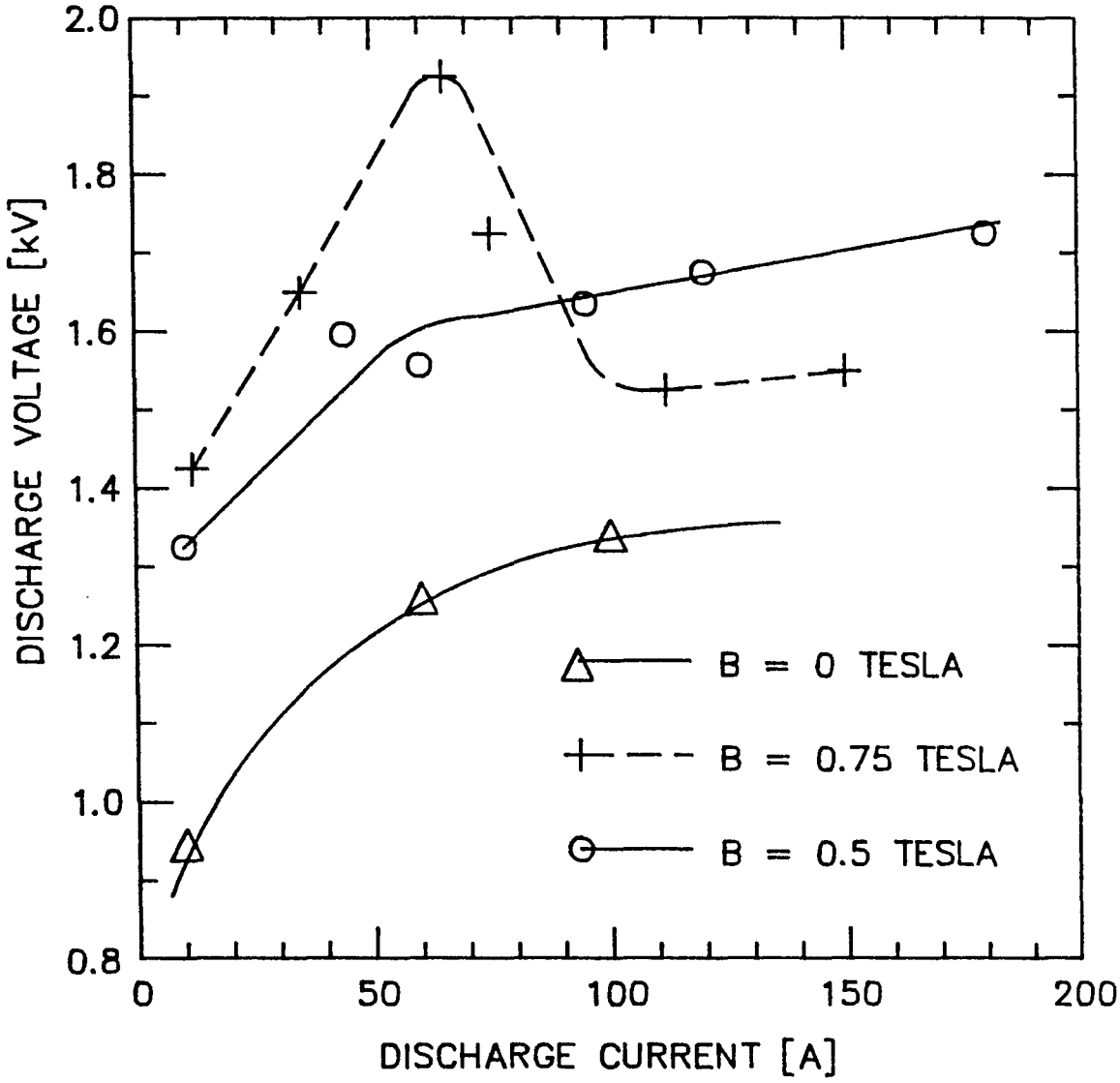


Figure 23. Experimental values of discharge voltage as a function of current in a 80% He - 20% $SF_6$ gas mixture at 8 torr. Note the reduction in the discharge voltage at larger values of discharge current.

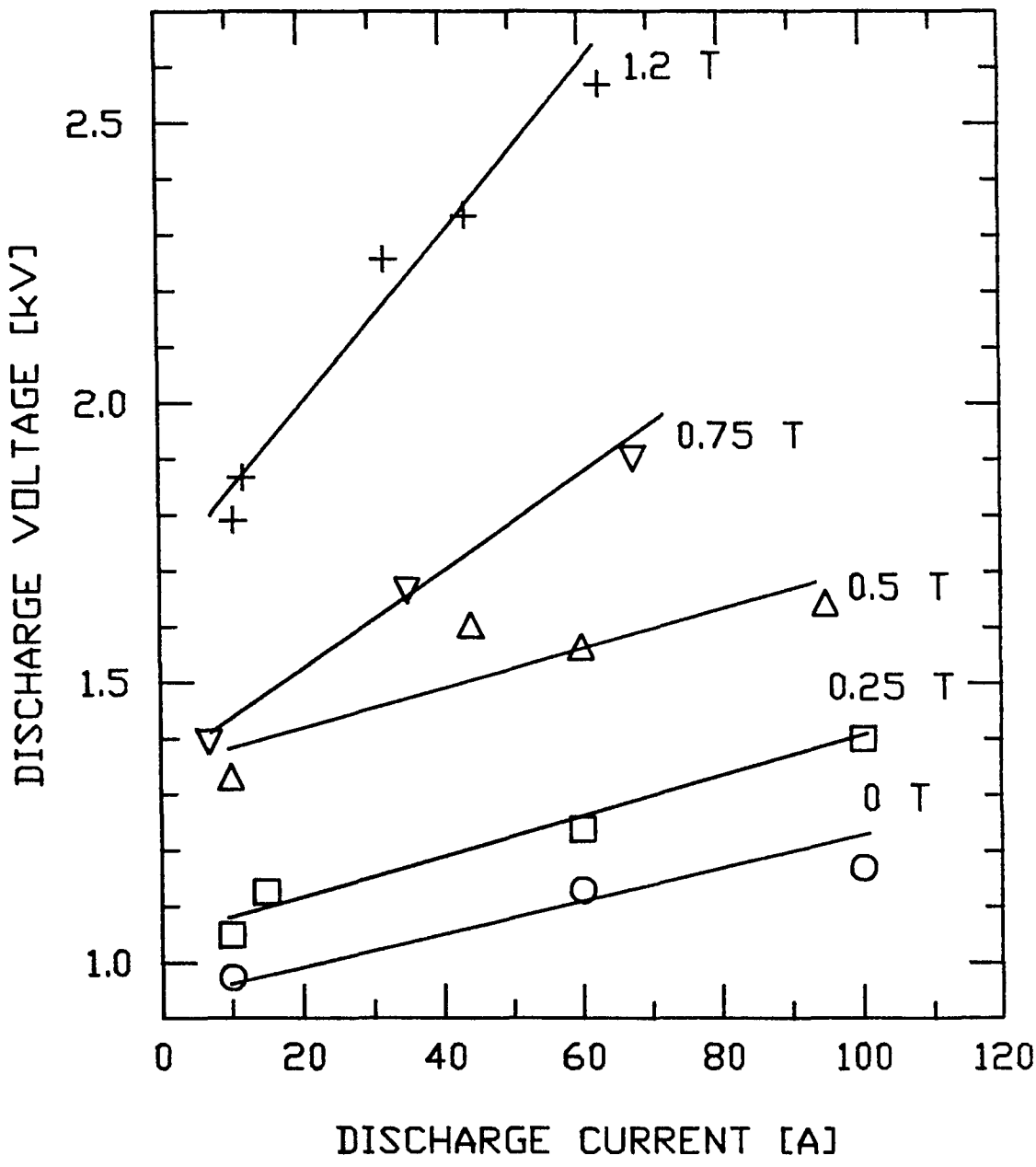


Figure 24. Experimental values of discharge voltage as a function of discharge current in an 80% He - 20% $SF_6$ gas mixture at 8 torr for various values of applied transverse magnetic field intensity.

The relationship between the discharge voltage and the applied magnetic field strength at constant discharge current was determined from Figure 24. These data are given as Figure 25 for discharge currents of 20, 60 and 100 amperes. The plot shows an initial increase in discharge voltage with respect to magnetic field (dV/dB) of approximately 0.4 kV/Tesla for the three values of current. This increases to a steady value which is dependent on the discharge current. Table IV gives the final values of dV/dB for the three values of current.

Table IV, experimental rate of rise of the discharge voltage with respect to applied magnetic field intensity for various current densities.

| I | dV/dB | B |
|---|---|---|
| 20 A | 1.6 kV/Tesla | 0.5 < B < .2 Tesla |
| 60 A | 2.3 kV/Tesla | 0.6 < B < 1.2 Tesla |
| 100 A | 2.6 kV/Tesla | 0.5 < B < 0.65 Tesla |

Besides measurements in He-$SF_6$, measurements in pure He were also performed.

Measurements in Pure He at a Constant Pressure

Figure 26 shows the measured quasi-steady-state voltage-current characteristics for the discharge in pure He with an applied transverse magnetic field. These measurements were made using He at a pressure of 8 torr and the same experimental setup used with He/$SF_6$. The error in this data is of the same magnitude as the He/$SF_6$ data. Unlike the He/$SF_6$ mixture, application of even the small transverse magnetic field of 0.03 Tesla

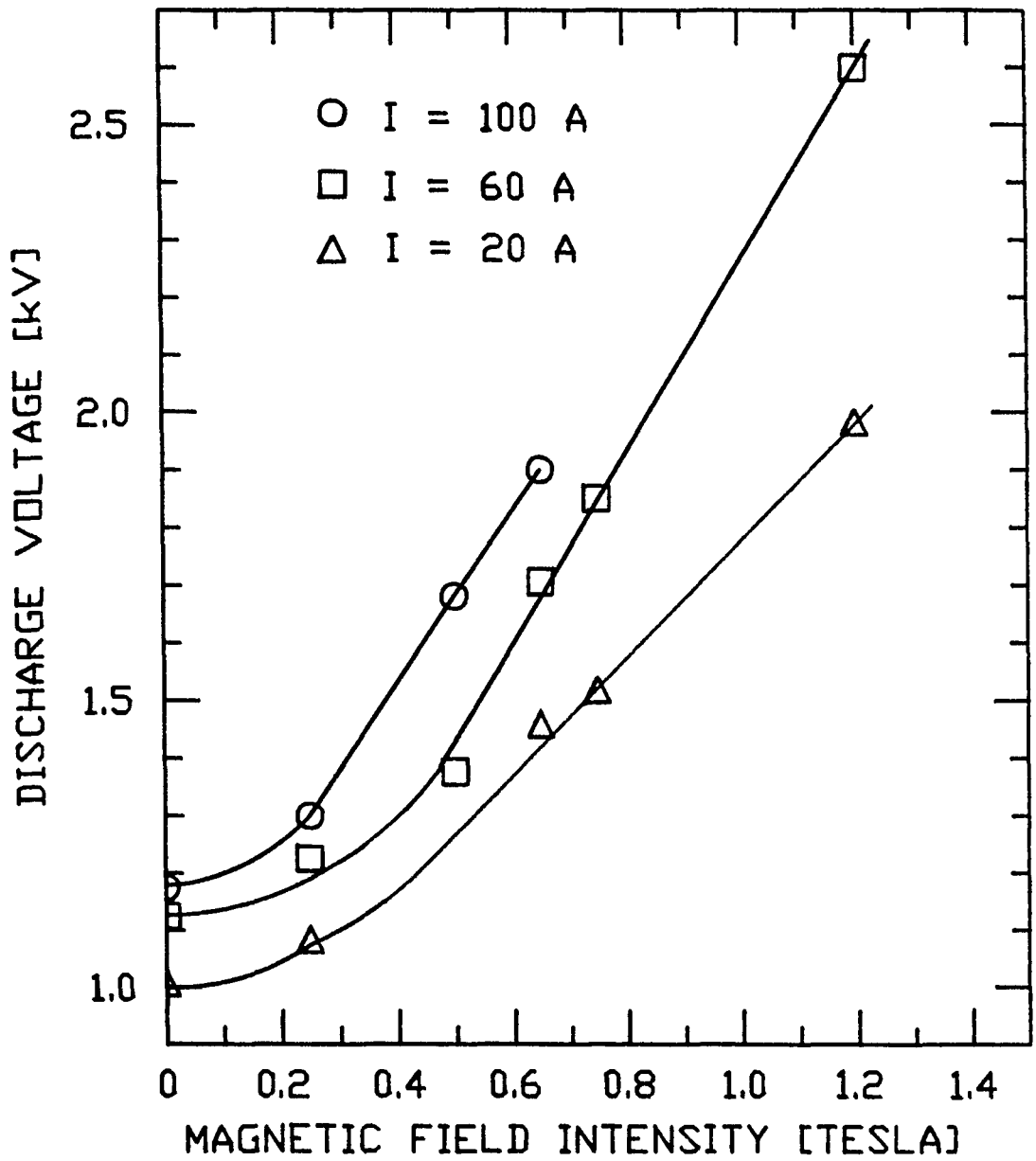


Figure 25. Experimental values of discharge voltage as a function of applied transverse magnetic field intensity in an 80% He - 20% $SF_6$ gas mixture at 8 torr for various values of discharge current.

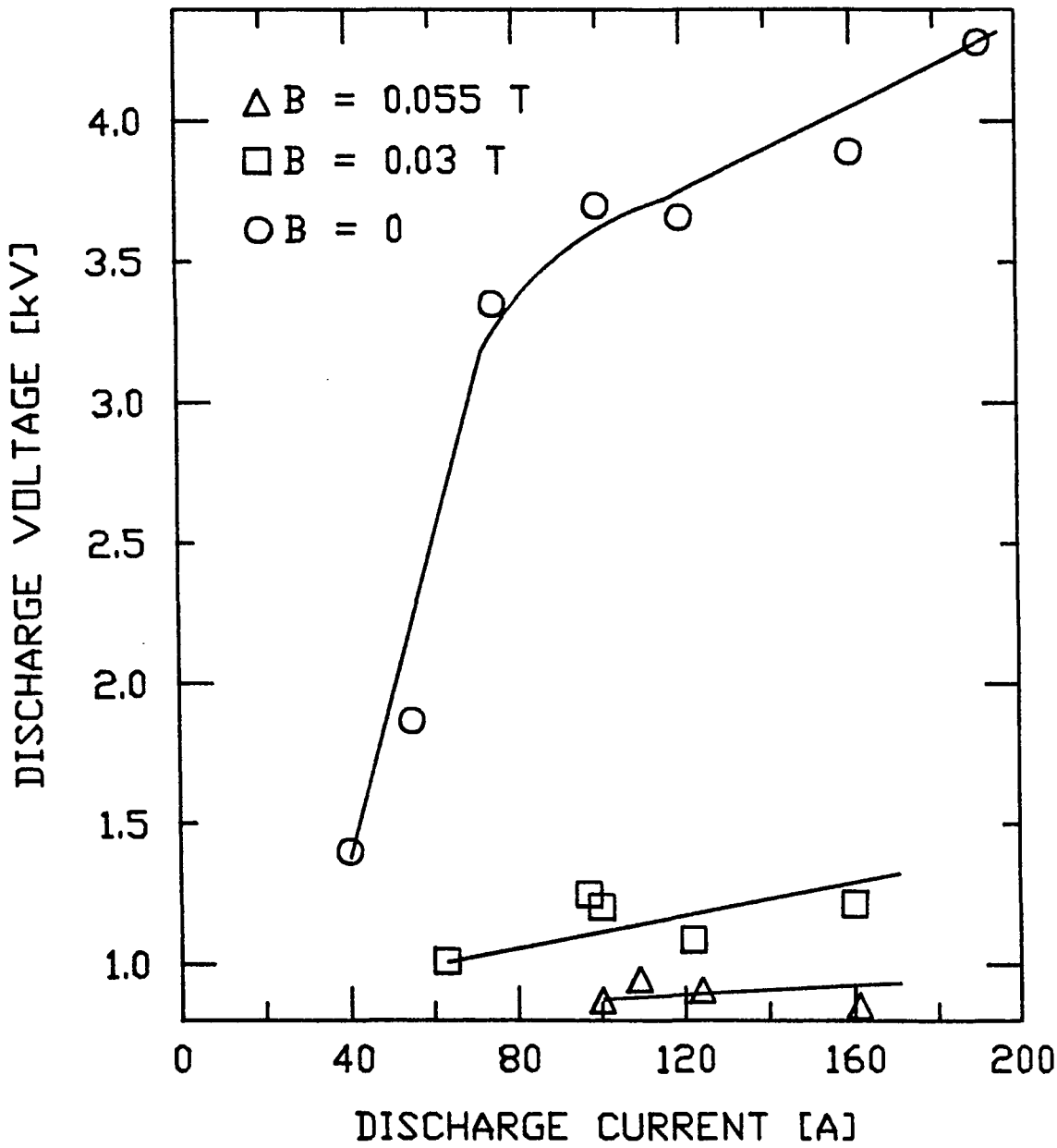


Figure 26. Experimental values of discharge voltage as a function of discharge current in pure He at 8 torr for various values of applied transverse magnetic field intensity.

causes a reduction in the discharge voltage. This is shown in Figure 27 which is a plot of the magnetic field versus the discharge voltage with a constant discharge current of 100 A. The discharge voltage with no magnetic field is 3700 V. This is reduced to approximately 1000 V when the applied magnetic field intensity is 0.03 Tesla.

Measurements of the Pressure Voltage Characteristics

To determine the operating pressure of the gas in the discharge chamber, pressure versus discharge voltage data were taken. Figure 28 shows the measured values of pressure versus sustaining voltage for $SF_6$, He and an 80% He - 20% $SF_6$ mixture. These data were taken by running the system in the self-breakdown mode. After the chamber pressure has been fixed the discharge current is set to 1 $A/cm^2$ by varying the gas pressure of the spark gap in the discharge circuit, and the discharge voltage is measured. Error of the data is approximately 15 percent. For consistency, the peak value of the discharge voltage during the conduction phase is recorded. This causes the voltages on these plots to seem larger than those used in the voltage-current and voltage-magnetic field measurements. Whereas the purpose of these graphs is to determine an operating point, to the right of the minimum sustaining voltage, for the system, this difference was deemed acceptable. While these curves should not be confused with Paschen curves (which are pd versus sparking voltage), the curves for $SF_6$ and the $SF_6$:He mixture

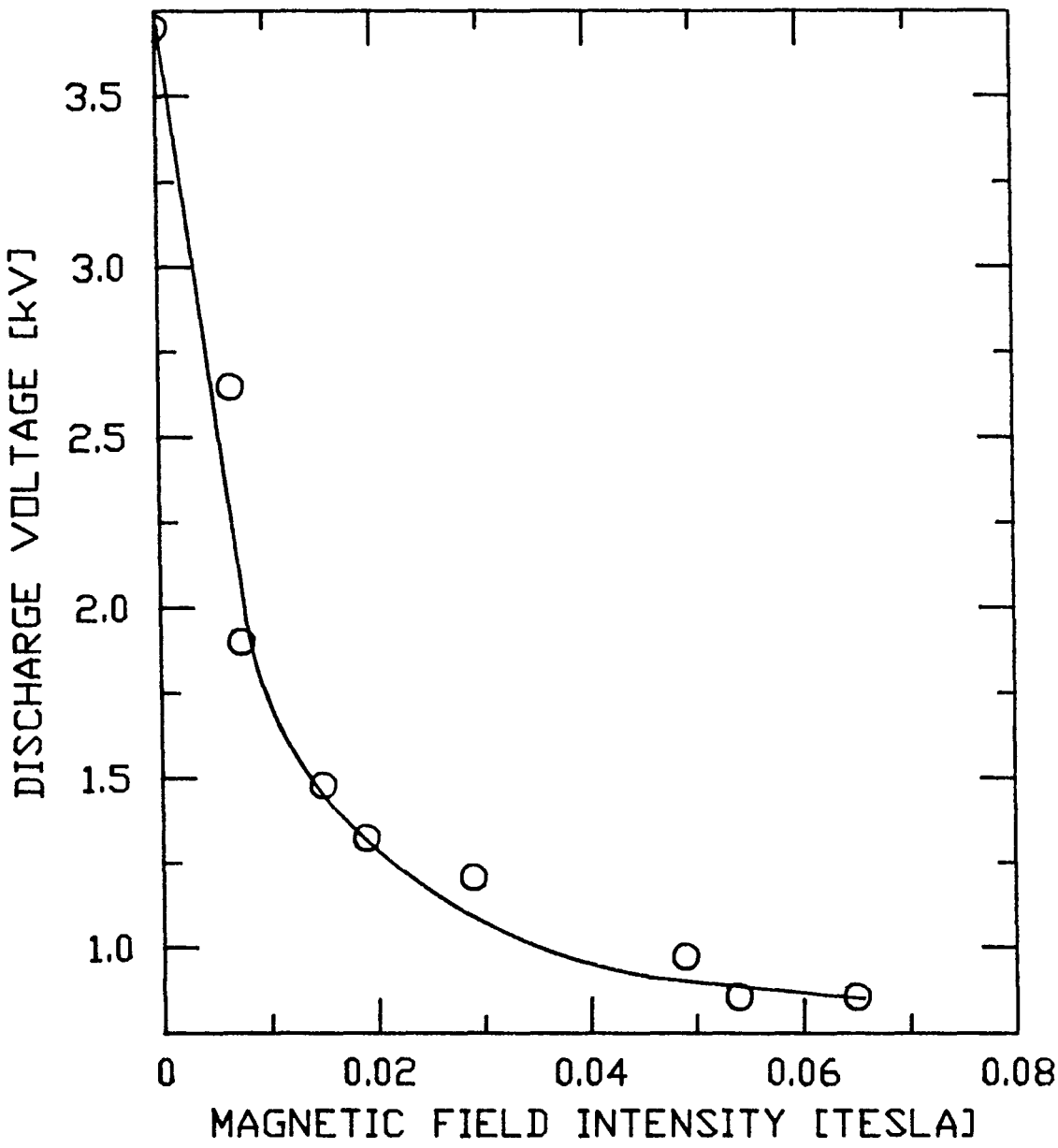


Figure 27. Experimental values of discharge voltage as a function of applied transverse magnetic field intensity in pure He at 8 torr with a discharge current of 100 A.

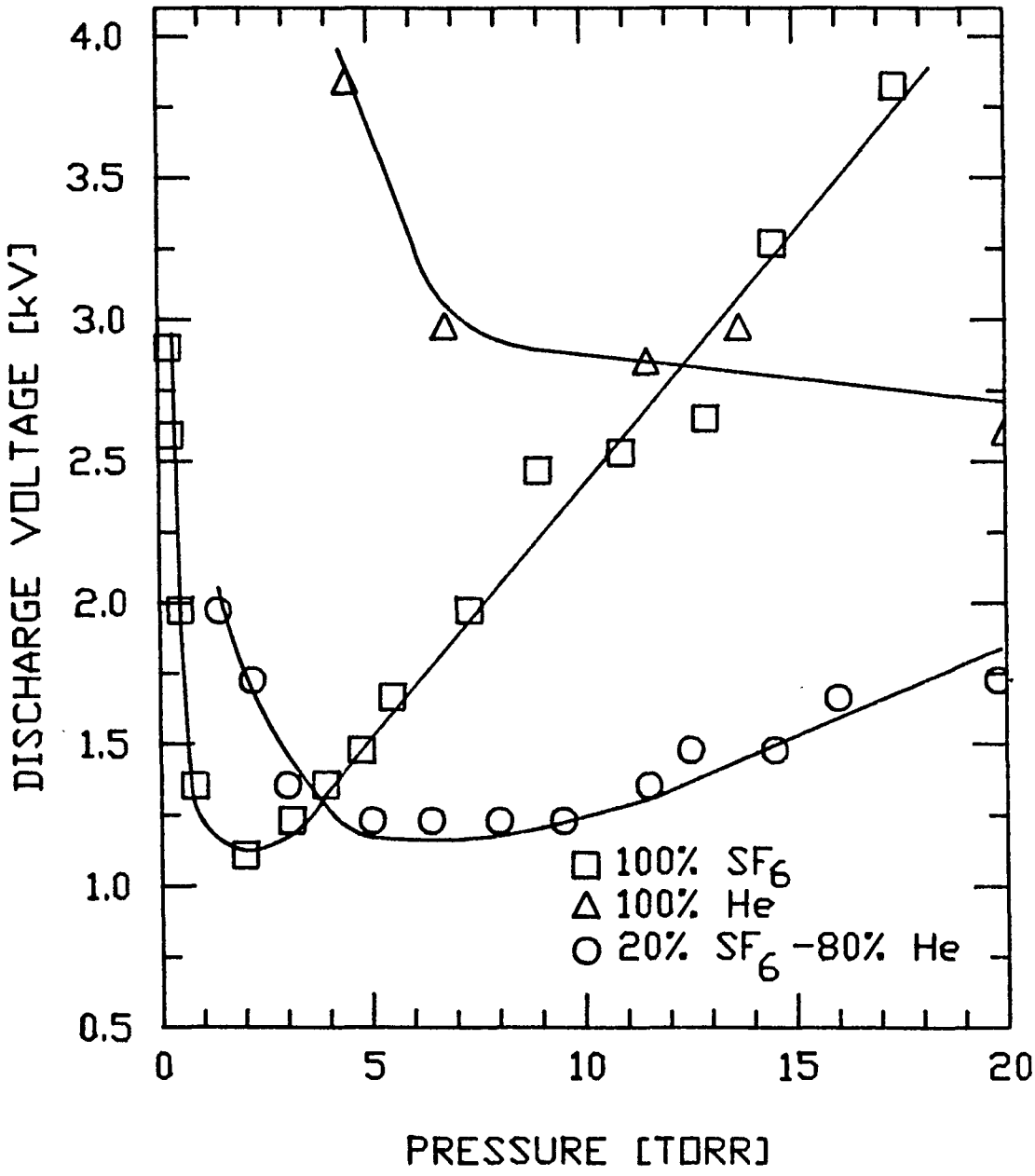


Figure 28. Experimental values of discharge voltage as a function of gas pressure for various gases. Discharge current is 100 A.

show the typical Paschen curve shape. There is a voltage minimum. The voltage increases as the pressure is either increased or decreased. The minimum voltage for $SF_6$ and the $SF_6$:He mixture are 1600 V and 1700 V respectively. The He curve does not show the rise on the high pressure side because of limitations in pressure measurements. It did rise at a pressure greater than 20 Torr.

# CHAPTER V
# DISCUSSION

Figure 29 shows the theoretical results for the positive column of a discharge in a 20% $SF_6$ - 80% He gas mixture. Two different models were used to arrive at these results (a) the equivalent electric field model and (b) the Monte Carlo model. Both of these models assume that the positive column voltage is not a function of current density. The value of the collision frequency ($3.3 \times 10^{10}$ $sec^{-1}$) used in calculating the equivalent electric field with the equivalent electric field model was taken from the Monte Carlo results (see Figure 12) at an E/N value of 90 Td. Figure 30 shows the experimental results in terms of reduced electric and magnetic field intensities. To convert the data of Figure 25, the positive column was assumed to extend over the region between the cathode and anode (2 cm) and the cathode fall voltage was not included. In general, the experimental data and theoretical results appear to be in agreement. At higher values of magnetic field, the rate of rise of voltage with respect to magnetic field intensity determined by the Monte Carlo method (1.8 kV/Tesla) falls between the experimental values for 0.2 $A/cm^2$ (1.6 kV/Tesla) and 0.6 $A/cm^2$ (2.3 kV/Tesla) and the

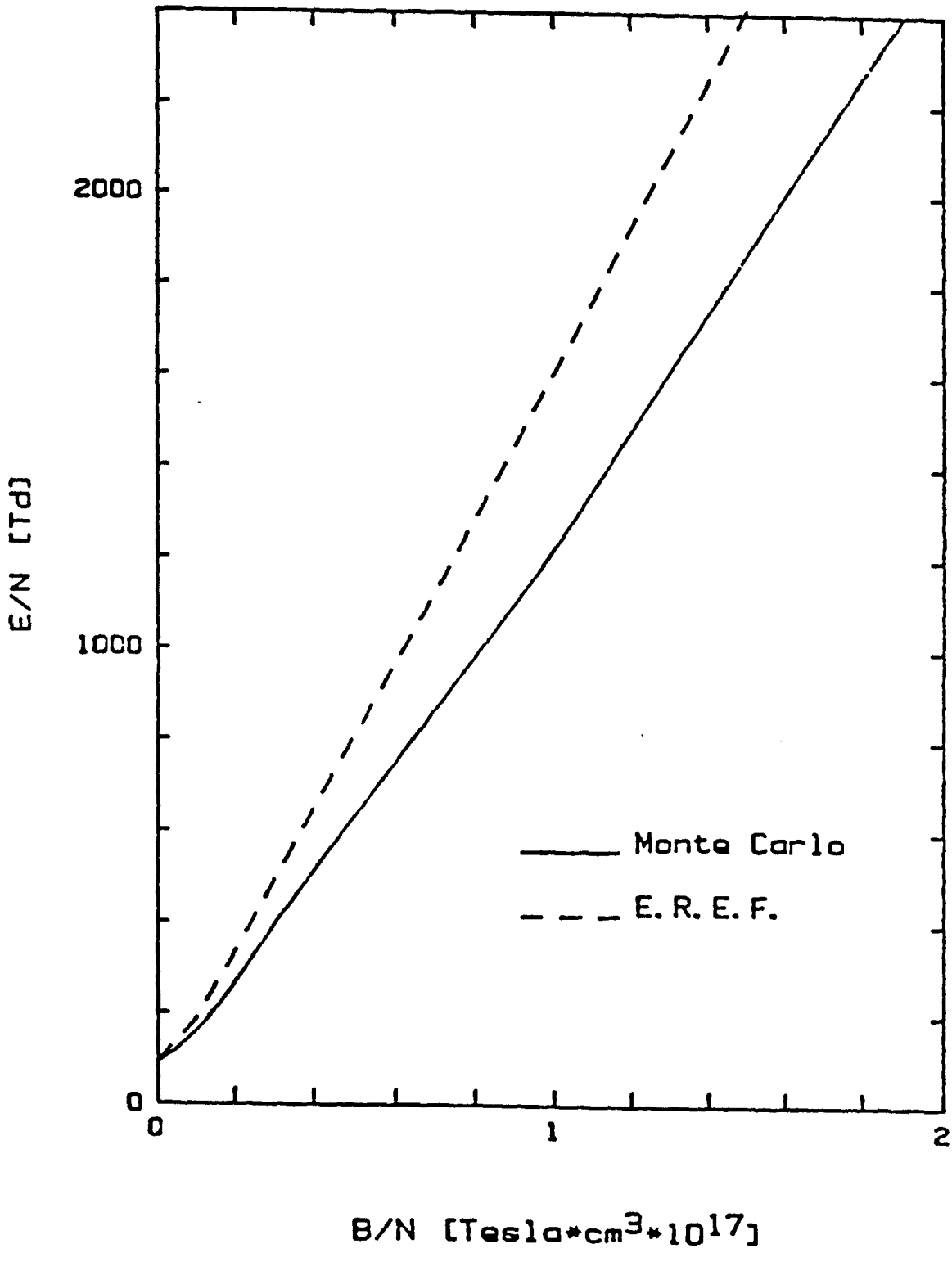


Figure 29. Reduced electric field intensity as a function of the reduced transverse magnetic field intensity as determined by the reduced electric field method and Monte Carlo method.

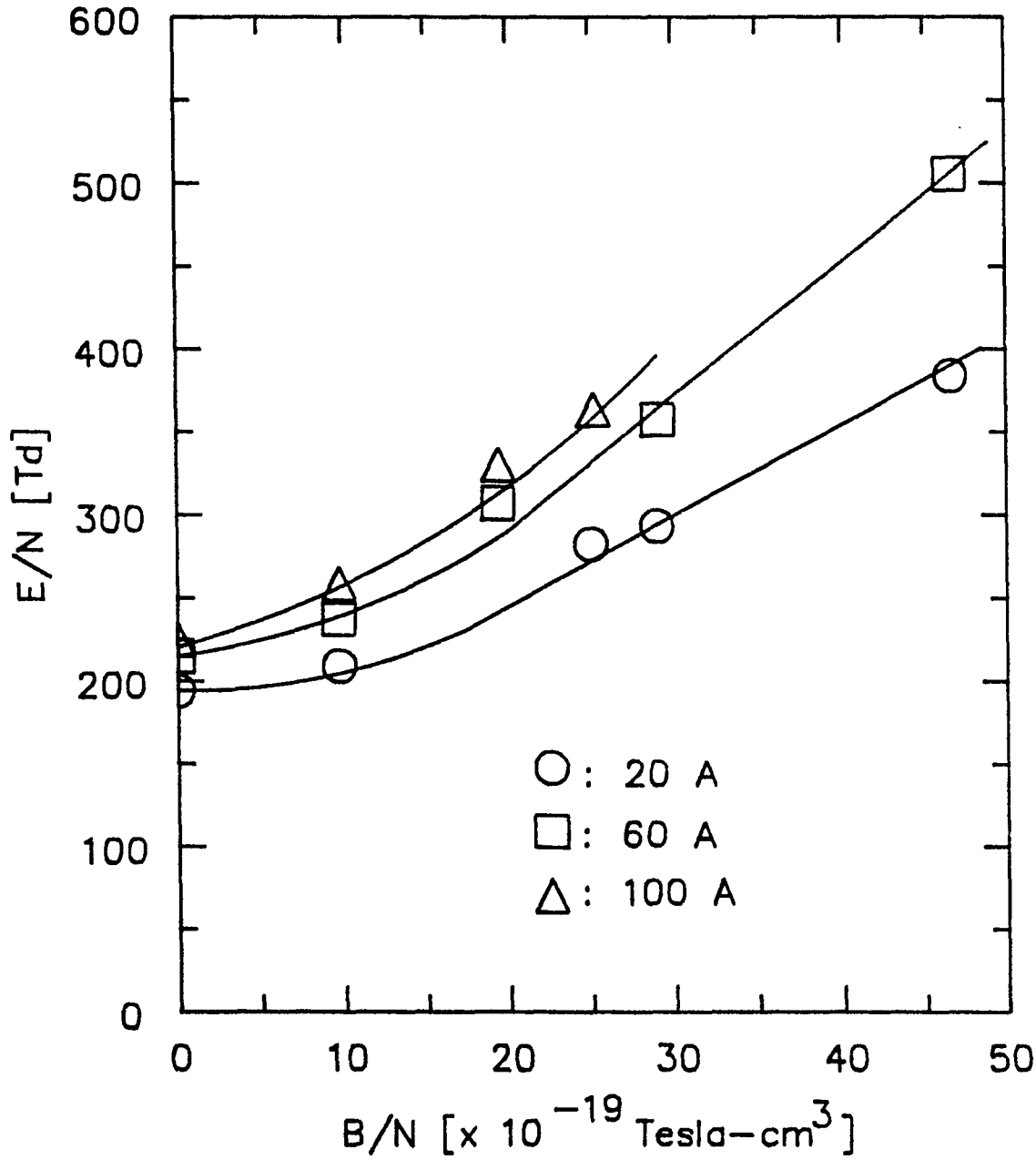


Figure 30. Reduced electric field intensity as a function of the reduced applied transverse magnetic field intensity in a 20% $SF_6$ - 80% He gas mixture at 8 torr. E/N was determined by assuming that the electric field was uniform over the 2 cm inter-electrode distance.

value calculated using the equivalent electric field method (2.7 kV/Tesla) is only four percent higher than the experimental value for 1.0 A/cm$^2$ (2.6 kV/Tesla).

The assumption that the cathode fall may be neglected can be used to explain the difference between the theoretical and experimental results at lower values of magnetic field intensity. As discussed in chapter I of this thesis, Figure 5 shows the relationship between the pressure and discharge voltage for zero applied transverse magnetic field and with a transverse magnetic field applied locally to the cathode fall region. When the discharge is operated to the left (low pressure side) of the critical point, application of a magnetic field causes a reduction in the cathode fall voltage. To the right of the critical point application of a magnetic field causes an increase in the cathode fall voltage. If the cathode fall voltage starts to the right of the critical point in Figure 5, and the magnetic field is increased, then the critical point moves to the right and the cathode fall voltage is reduced. This can be seen by considering the difference the experimental results at 0.2 A/cm$^2$ and the Monte Carlo results. At a value of magnetic field intensity of 0.65 Tesla the cathode fall voltage would become negative according to our simple model for the positive column. For this reason, other collisional processes must be added to the model. At higher current densities with corresponding higher electron densities a

process which should be considered is recombination, which is generally dependent on $n_e$. Adding a recombination term to the electron rate equation changes the form to

$$dn_e/dt = -k_a n_e N_a + k_i n_e N_o - k_r n_e^2 \quad . \qquad (32)$$

The other unexplained results in the $He/SF_6$ mixture is the reduction, vice an increase, of the discharge voltage as the magnetic field intensity or current density is increased. This reduction takes two different forms. In the first case the voltage changes from several kilovolts to some tens of volts (glow to arc transition). One reason the arcing is occurring may be the instabilities caused when the cathode fall distance decreases and the electric field strength in the cathode fall increases when the current density [6] or magnetic field intensity [11] are increased. In the second reduction (of the discharge voltage) type the discharge voltage is lower, but still of the same order, than that of a discharge with a lower magnetic field and the same current density.

One possible explanation which would account for the gradual reduction of the discharge voltage with increases in current density and magnetic field intensity may be found in Figure 5. While the system is operating at low magnetic field strength and low current density, the cathode fall voltage lies on the right of or near the

critical point. At larger values of magnetic field strength and current density the operating point has moved to the left of the critical point and the application of a magnetic field effectively decreases the cathode fall voltage.

The results obtained with helium show the same type of effect used to control the gamitron switch [16]. When moderate magnetic fields are applied to the discharge its voltage is decreased. This is an indication that the discharge is operating to the left of the critical point of Figure 5. One explanation for the process on the pressure side of the critical point in Figure 5 is that at this pressure with no magnetic field, the cathode fall - negative glow regions have expanded to the point where they occupy the entire inter-electrode gap which causes the voltage to rise. However, the discharge has not reached the point of obstruction. The pressure-distance product, $pd_c$, for He with a Al cathode and no applied magnetic field is 1.32 Torr-cm while for $O_2$, which is an attacher gas, it is 0.24 Torr-cm [2]. When the transverse magnetic field is applied the cathode fall distance in He is reduced. This causes the inter-electrode distance to be greater than the cathode fall - negative glow distance and the voltage is reduced.

Switch Operation

If the $He/SF_6$ discharge is to be used as an opening switch, one possible configuration would be to operate the

switch on the load line shown in Figure 31. The switching operation is performed by initiating the discharge with zero magnetic field to a voltage of 1200 V and current of 100 A. A transverse magnetic field of 1.2 Tesla is applied and the voltage current characteristics move up the load line to a voltage of 1800 V with a current of 10 A. This would represent an increase in the discharge resistance from 12 Ω to 180 Ω.

The He discharge may be operated as an opening switch by initiating the discharge with a transverse magnetic field intensity equal to 0.06 Tesla, a voltage of 800 V and current of 160 A (see Figure 32). The magnetic field is removed and the voltage-current characteristics move up the load line to 3200 V and 70 A. This would represent an increase in the discharge resistance from 5 Ω to 46 Ω.

One of the problems in using a cold cathode discharge as a switch is the relatively large forward voltage drop of several hundred volts to several kilovolts. One method of reducing this is by means of a hollow cathode. A hollow cathode was constructed and tested. Although there was a reduction in the discharge voltage in He, only preliminary results were obtained and further investigation is required. Additionally, hollow cathode discharges are capable of sustaining a glow discharge at much higher current densities without changing to an arc [26].

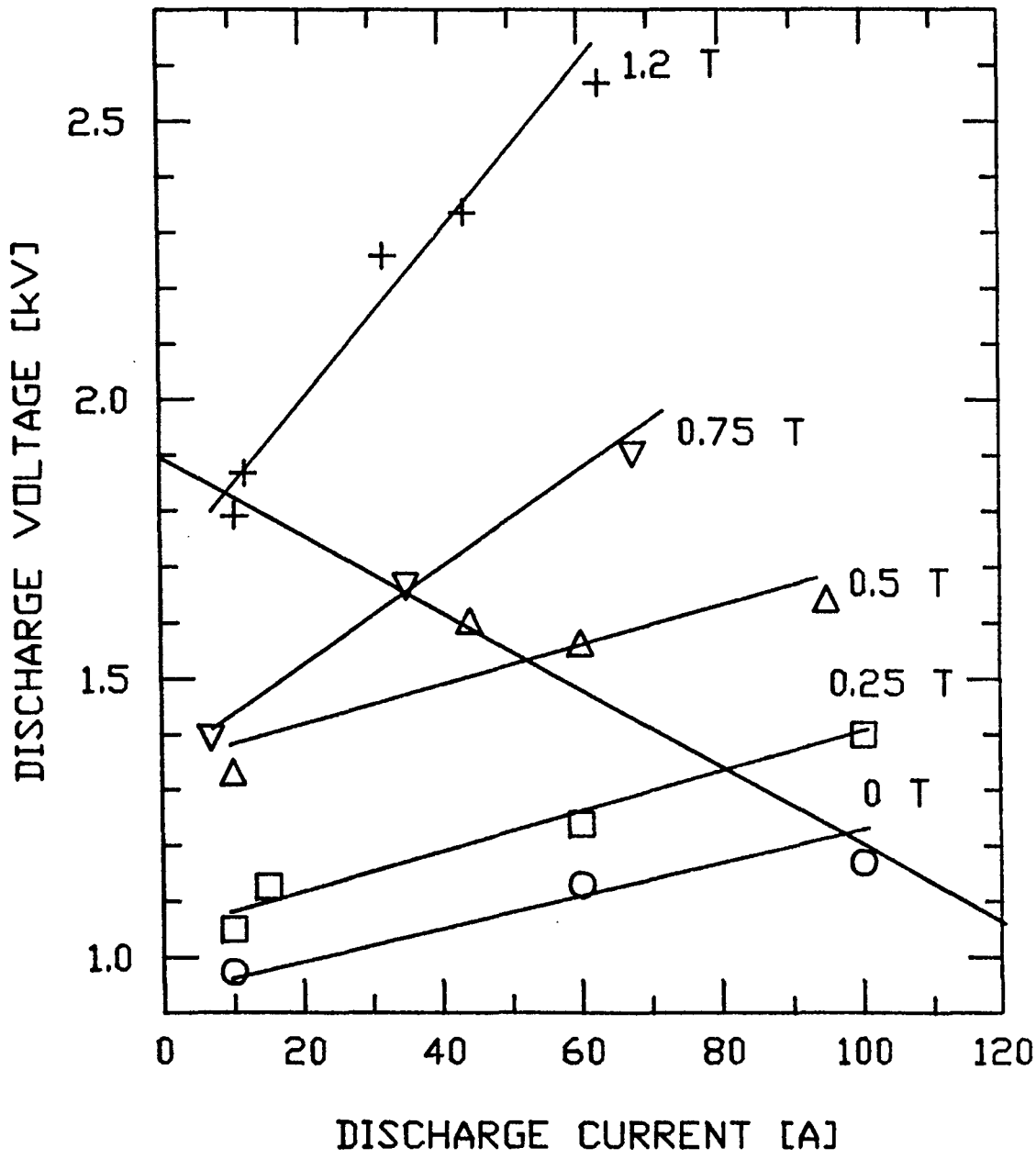


Figure 31. Experimental values of the discharge voltage as a function of the current in an 80% He - 20% $SF_6$ gas mixture at 8 torr with a proposed load line.

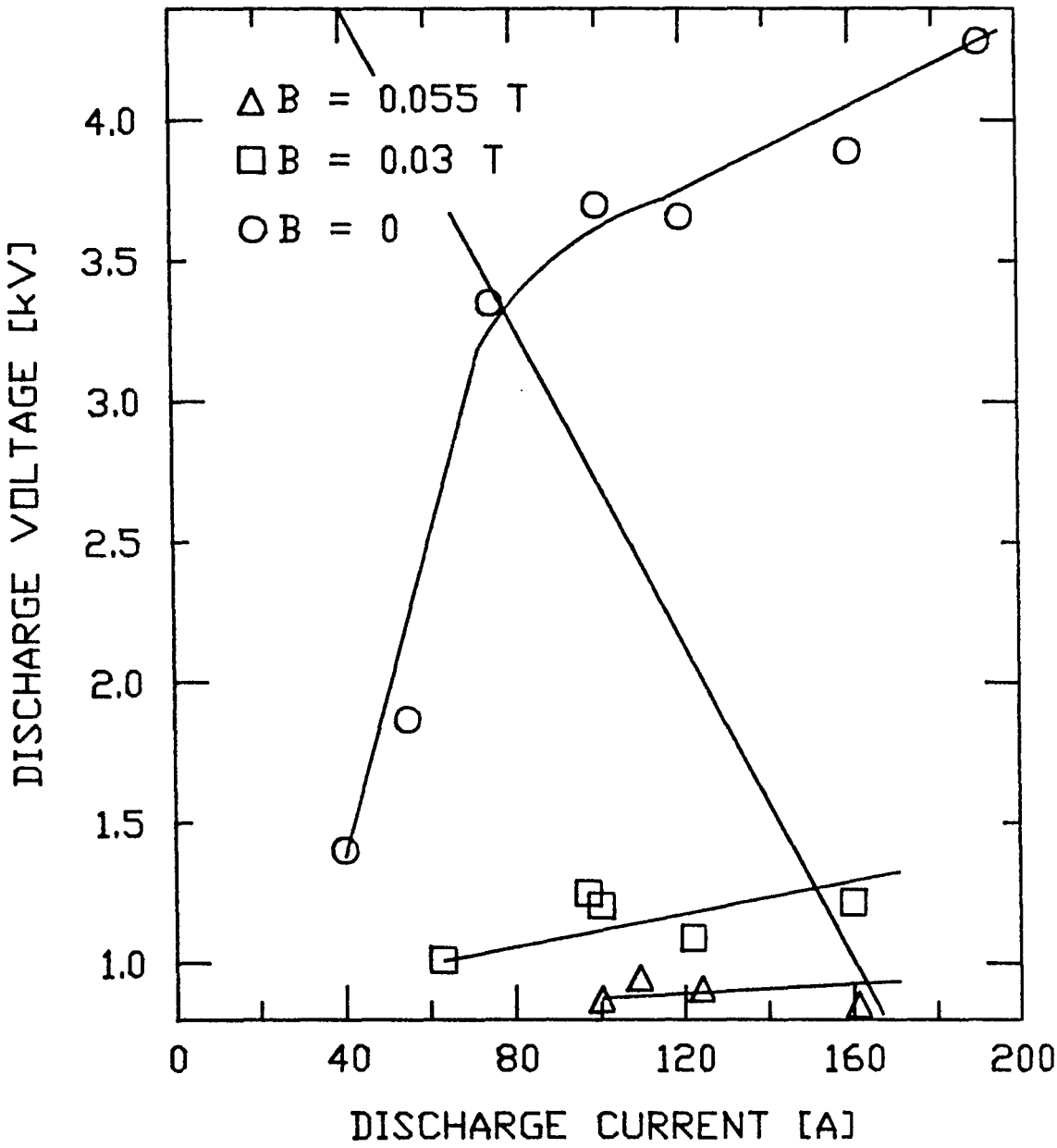


Figure 32. Experimental values of the discharge voltage as a function of the current in pure He at 8 torr with a proposed load line.

Summary

The effect of a transverse magnetic field on a glow discharge in a 80% He. - 20% $SF_6$ gas mixture at a pressure of 8 torr was studied. The measured increase in the discharge voltage with respect to increases of the applied transverse magnetic field ranged between 1.6 kV/Tesla and 2.6 kV/Tesla. These values are consistent with the increase in the positive column electric field intensity predicted using Monte Carlo calculations [20]. At current densities greater than 1 $A/cm^2$ and magnetic field intensities greater than 0.65 Tesla there was a departure from the predicted values. The use of this gas mixture and pressure range as an opening switch is limited due to the large magnetic field required to obtain a reasonable increase in the discharge impedance.

In He at a pressure of 8 torr, the application of a transverse magnetic field decreases the discharge voltage. At 1 $A/cm^2$ the discharge voltage is reduced from 3700 V to 1000 V by applying a transverse magnetic field of 0.03 Tesla. A switch using this gas and pressure range could be used as an opening switch rather efficiently due to the low magnetic field requirements. To open this switch the magnetic field would have to be reduced or counter-pulsed.

Future work in this area is possible in two basic areas. These two areas are the study of the transient

properties of the discharge and the properties of the cathode fall region. The steady state data could be used to investigate a system in which a pulsed magnetic field is applied to a static discharge thus affecting an opening switch. The effects of the cathode fall could be investigated to determine methods of controlling its properties. The hollow cathode effect could be investigated to reduce the discharge voltage and increase the current density.

# APPENDIX A
# EXPERIMENTAL SETUP

This appendix describes specific details about the experimental setup, it's construction and the estimates made in determining the electronic parameters of some of the system components. The basic components which will be discussed will be the magnetic field coil, discharge chamber and the capacitive voltage divider.

## THE MAGNETIC FIELD COIL

The magnetic coil is a 100 turn coil of 12 gauge solid copper wire with 600 V insulation which is separated into four concentric layers. A sheet of 10 mil mylar is placed between each layer to eliminate layer to layer breakdown. The inductance for the coil may be estimated using the following equation [27]:

$$L = \mu_o N2A/\{h[1+0.9(r/h)+0.32((b-a)/r)+0.84((b-a)/h)]\} \quad (33)$$

where N is the number of turns (100), A is the cross-sectional area of the solenoid (0.0.117 $m^2$), h is the axial length of the solenoid (0.075 m), r is the radius to the center of the winding (0.061 m), (b-a) is the thickness of the winding (.012 m) and $\mu_o$ is the magnetic permeability of free space. Using this formula and the dimensions of the coil a theoretical value is

calculated for the inductance equal to 1010 μH which is consistent with the measured value of 970 μH.

The magnetic field intensity on the axis of the coil, in Tesla, was calculated using the following equation [28].

$$B_z(z)=(\mu_o NI/2h)[\{(h-z)\ln\{(b+\sqrt{(b^2+(h-z)^2)})/(a+\sqrt{(a^2+z^2)})\}+ \{z\ln\{(b+\sqrt{(b^2+z^2)})/(a+\sqrt{(a^2+z^2)})\}\}]/(b-a) \quad (34)$$

where N is the number of turns, $\mu_o$ [H/m] is the permeability of free space, z is the distance along the axis from one end of the coil, h is the length of the coil, a is the inner radius and b is the outer radius of the coil in meters. Figure 33 is a plot of the variation of the calculated magnetic field intensity as a function of position along the axis of the coil when I = 1000 A. The relationship between the magnetic field intensity at the center of the coil and the current is

$$B_z = 8.8 \times 10^{-4} \ I \ [\text{Tesla}]. \quad (35)$$

This value varies by approximately 25% from the center of the coil to each end. The measured value of the magnetic field at the center of the coil with 20 A of current is 120 gauss. This is in relative agreement with the value of 176 gauss calculated using equation 34.

Electrode Finishing Process

The cathode is sanded to a "brushed" finish by first sanding out any pits or scratches using 400 grit sandpaper and finishing it with 600 grit sandpaper. A similar finish is obtained on the harder stainless steel by first

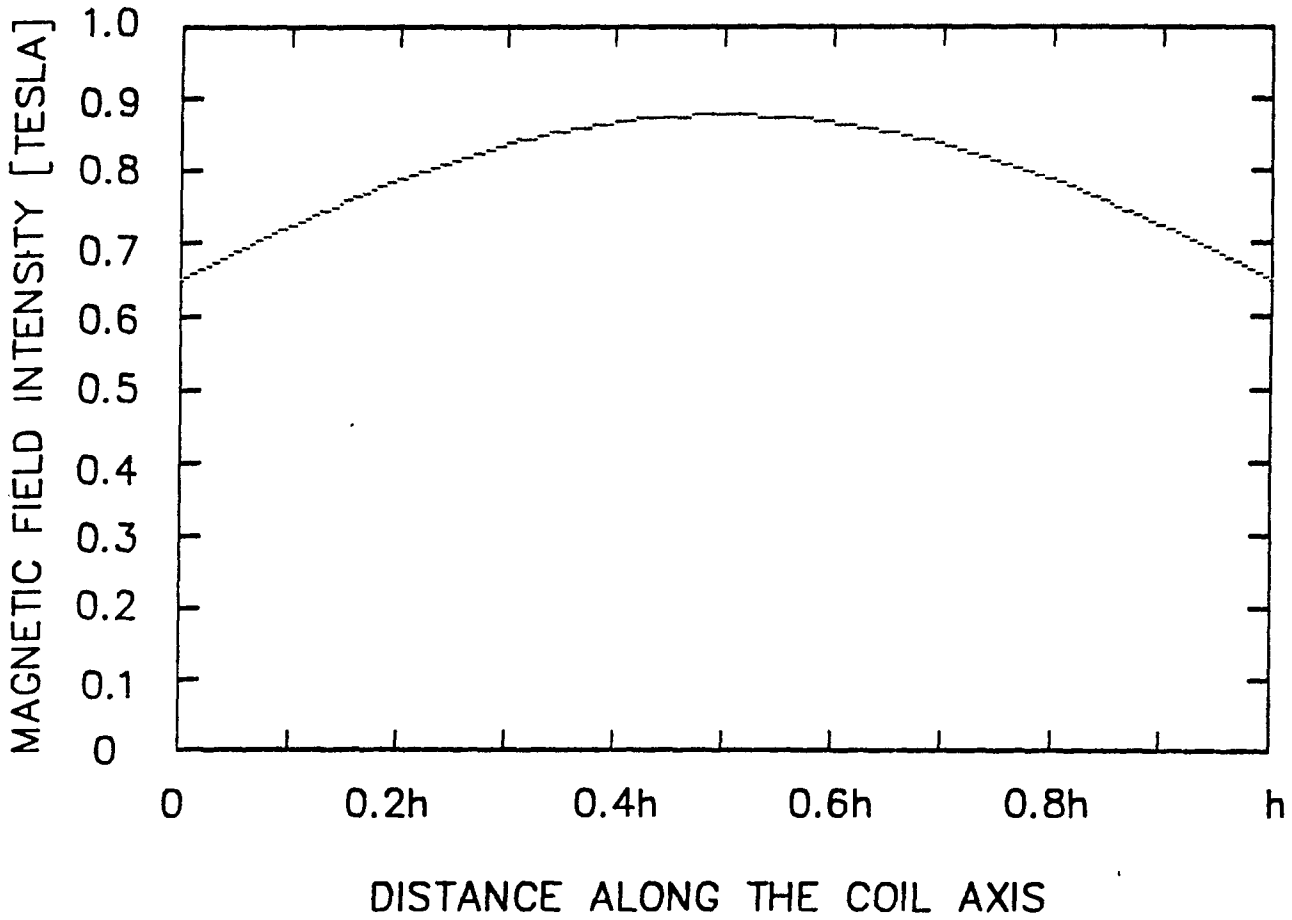


Figure 33. Calculated magnetic field intensity along the center of the coil. I = 1kA.

sanding out the pits with 150 grit sandpaper followed successively by sanding with 320 grit and 400 grit. The metal and teflon material is then cleaned with acetone and the acrylic parts are cleaned with soapy water and allowed to dry. After the system has been assembled and pumped down for several hours the electrodes are "pulsed cleaned" by generating a low-current (tens of amperes) pulsed helium discharge in the system. This removes any oxides which may be on the conducting surfaces. After several thousand shots in the $SF_6$:He mixtures the cathode and the anodes become coated with fluorine compounds and pits in the surfaces start to form. These pits eventually cause current filaments which lead to arc type discharges and are cause to disassemble the system and refinish the electrodes.

The Capacitive-Resistive Voltage Divider

Figure 34a is an isometric drawing of the capacitive voltage divider used as part of the experimental setup. Figure 34b is the equivalent circuit of the divider network. The resistor $R_1$ is the resistor that is mounted in the assembly (e.g., the 18 kΩ resistor), and $R_2$ is a terminating resistor (e.g., 50 Ω). The capacitor $C_1$ is the capacitance between the inner conductor and the metal foil, and $C_2$ is the capacitance between the metal foil and the aluminum housing. Both of these may be calculated using the following equation:

$$C = 2\pi \varepsilon l / \ln(b/a) \qquad (36)$$

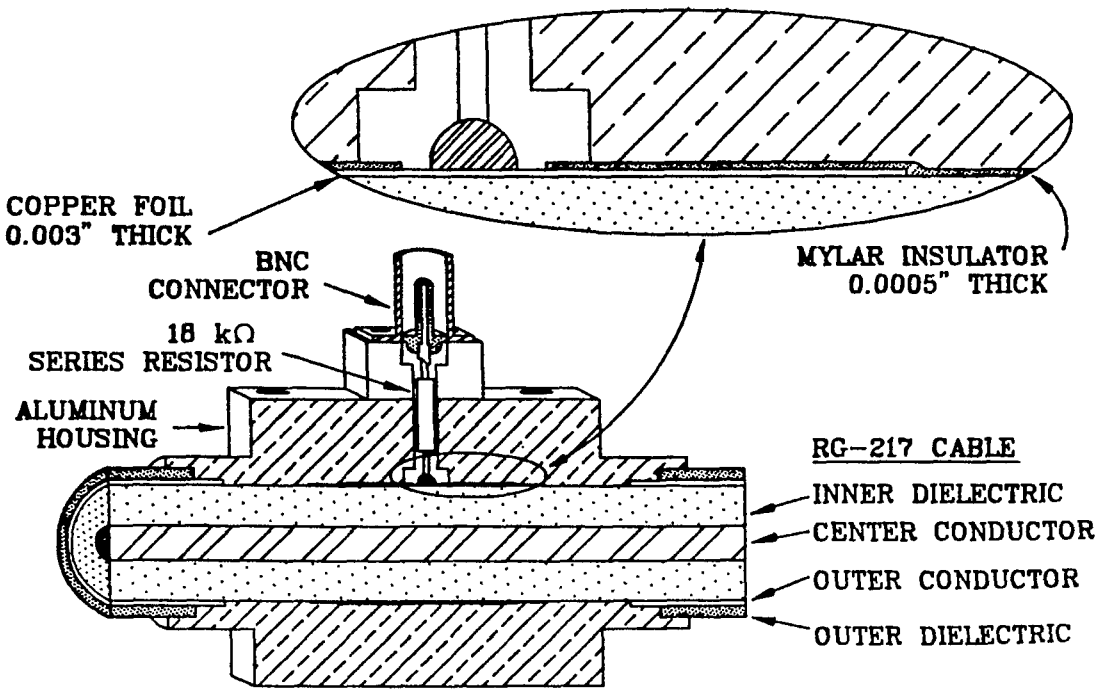


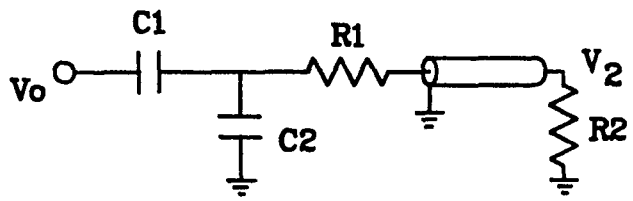


Figure 34. (a) Isometric and (b) schmatic diagram of the capacitive voltage divider network.

where l is the length of the capacitor, b is the outer diameter and a is the inner diameter. Substituting the appropriate values leads to a value for $C_1$ equal to 2.2 pF. Because non-uniform spacing between the foil and the aluminum housing $C_2$ was calculated from the divider ratio A and the known values of $C_1$, $R_1$ and $R_2$. Its value was calculated to be 370 pF. It can be shown that the transfer function of the network is

$$\frac{V_2(S)}{V_o(S)} = \frac{R_2 C_1 S}{1 + (C_1 + C_2)(R_1 + R_2)S} \tag{37}$$

where $V_o(S)$ is the potential of the center conductor of the cable and $V_2(S)$ is the potential of the signal at the test equipment. The time response of the network to a step signal of magnitude $V_o$ is

$$V_2(t) = V_o A\, e^{(-t/\tau)} \tag{38}$$

where

$$A = (R_2C_1)/(R_1 + R_2)(C_1 + C_2) \tag{39}$$
$$= 1/68100$$

and

$$\tau = (R_1 + R_2)(C_1 + C_2). \tag{40}$$
$$= 6.6 \times 10^{-6} \text{ sec}$$

The factor $e^{-(t/\tau)}$ introduces an error to the output signal which is a function of the pulse length. This factor is known as droop. It is normally given in percent per microsecond. This network has a droop of 15 %/μsec.

If the signal is more complex than a step signal, the transfer function introduces other errors. This can be

seen by considering the response of a capacitive-resistive voltage divider to the following waveform

$$V_{in}(t) = V_o( u(t) - Bu(t-T) - (1-B)u(t-2T)). \quad (41)$$

This describes a square pulse T seconds wide with a magnitude of $V_o$ followed by pulse $(1-B)V_o$ in magnitude for T seconds. Ideally the output of a voltage divider would be A times the input function for all t. The actual response of the network is

$$V_{out}(t) = V_o\ A\ e^{-t/\tau}[u(t) - B\ e^{T/\tau}u(t-T) - (1-B)e^{2T/\tau}u(t-2T)]. \quad (42)$$

Assuming $T = 0.1\tau$, $A = 1/1000$, $V_o = 2.5$ kV and $B = .75$, the output of the network is a pulse which falls off exponentially to 90% of its ideal value in T seconds. At T the value of the output is 0.375 V vice its ideal value of 0.625 V (a 40% difference). At 2T the value of the output is -0.274 V vice the correct value of zero volts. However the waveform maintains its temporal characteristics in a time frame short compared to $\tau$. The two waveforms are shown in Figure 35. The overall effect is an effective shift in the zero voltage level of the signal which is related to the previous value of the function.

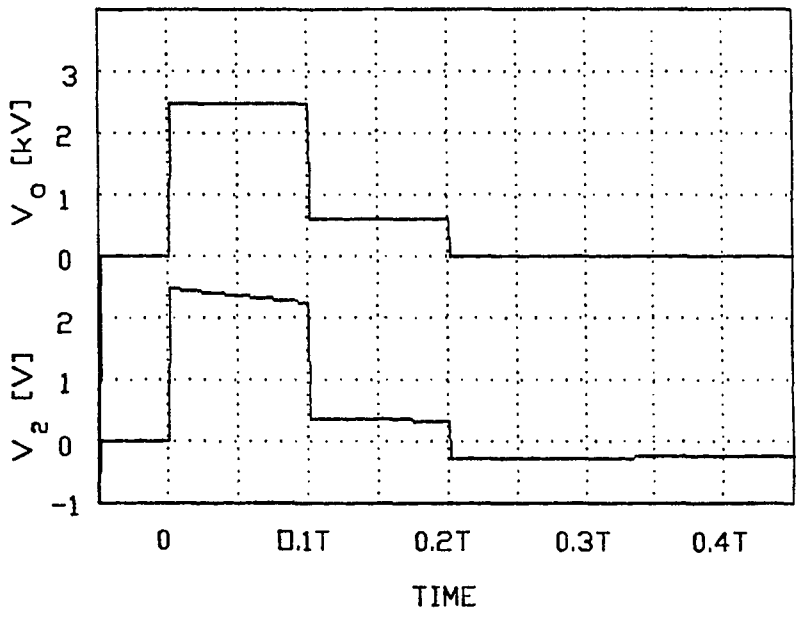


Figure 35. Theroretical input (upper) and output (lower) waveforms for a capacitive-resistive voltage divider network.

## APPENDIX B
## THE INFLUENCE OF MAGNETIC FIELDS ON THE CHARGE CARRIERS IN A GLOW DISCHARGE

When an electron is in the region of a magnetic field it will travel in a helical path around a guiding center which is parallel to the direction of the applied magnetic field. While motion of the electron in the direction of the magnetic field is not affected, the motion in the plane perpendicular to the applied field is that of a circle. The radius of this circular path is known as the larmor radius which is given by Equation (44). The frequency at which it travels this path, known as the cylclotron frequency, is given by Equation (43).

$$\omega_c = eB/m_e \qquad (43)$$

$$r_L = v_\perp / \omega_c = m_e v_\perp / eB \; . \qquad (44)$$

It should be noted that the frequency of the rotation is only a function of the electron charge to mass ratio and the applied magnetic field while the radius is a function of the perpendicular velocity component and the cyclotron frequency.

If a constant electric field is present, as in the positive column or prior to breakdown, the electrons follow the path given by Equations (45), (46) and (47) [20].

$$x(t) = x_o + v_{xo}t \qquad (45)$$

$$y(t) = y_o + (v_{yo}\sin\omega_c t)/\omega_c + v_{zo}(1 - \cos\omega_c t)/\omega_c + (E/B)[t-(\sin\omega_c t)/\omega_c] \qquad (46)$$

$$z(t) = z_o +(v_{zo}\sin\omega_c t)/\omega_c + [E/B\omega_c^2 - v_{yo}/\omega_c]\cos\omega_c t - E/B\omega_c^2 + v_{yo}/\omega_c \qquad (47)$$

where the magnetic field, $\underline{B}$, is in the positive x direction and electric field, $\underline{E}$, is in the positive z direction. These three equations represent a cycloid path in the yz-plane, in which the electron moves in the positive y direction with an $\underline{E}x\underline{B}$ drift velocity equal to the ratio of the electric field strength to the magnetic field strength. Additionally, the electron continues to drift in the x direction at $v_{xo}$. The maximum distance traveled by the electron in the direction of the electric field, $z_{max}$, is given by Equation 48.

$$z_{max} = z_o + (-E/B\omega_c + v_{zo}/\omega_c). \qquad (48)$$

If an electron starts at the cathode of a planar system it will return to the cathode if two conditions are met. The first condition is that the inter electrode distance is greater than the critical value given in Equation 48. The second condition is that the electrons do not collide during the time given by $1/\omega_c$. This condition is be met if $\nu_c/\omega_c << 1$. The solution of the momentum balance equation for the electron drift velocities in the x and y directions is given as Equations 50 and 51 respectively.

$$m_e d\underline{v}/dt = -e[\underline{E} + \underline{v} \times \underline{B}] - m_e \underline{v} \nu_c \qquad (49)$$

$$v_x = (E/B)(\nu_c/\omega_c)/[1 + (\nu_c/\omega_c)^2] \qquad (50)$$

$$v_y = -(E/B)/(1 + (\nu_c/\omega_c)^2 \qquad (51)$$

Again $\underline{B}$ is in the positive-x direction and $\underline{E}$ is in the positive-z direction. When $\nu_c/\omega_c << 1$, $v_y$ approaches $-E/B$ and $v_x$ approaches zero. When $\nu_c/\omega_c >> 1$, $v_y$ approaches $-E\omega_c^2/B\nu_c^2$ and $v_x$ approaches $Ee/m_e\nu_c$. In the first case the plasma is collisionless and the drift velocity is simply the $\underline{E}\times\underline{B}$ drift contained in Equation (46). In the second case the $\underline{E}\times\underline{B}$ drift is reduced by a factor of $\omega_c^2/\nu_c^2$ and the drift velocity in the direction of the electric field approaches that of no magnetic field.

## LIST OF REFERENCES


[1] R. G. Fowler, In An Introduction to Discharge and Plasma Physics, Edited by S. C. Haydon, Armidale, N. S. W., Australia, U. of New England, 1964.

[2] E. Nasser, Fundamentals of Gaseous Ionization and Plasma Electronics, New York, Wiley-Interscience, 1971.

[3] J. D. Cobine, Gaseous Conductors, Theory and Engineering Applications, New York, Dover Publications, Inc., 1958.

[4] B.N.Chapman, Glow Discharge Processes and Plasma Etching, New York, John Wiley & Sons, 1980.

[5] A. von Engel, Electric Plasmas: Their Nature and Uses, New York, Taylor & Francis Inc., 1983.

[6] D. K. Doughty, E. A. Den Hartog, and J. E. Lawler, "Optogalvanic Measurements of Gas Temperature in the Cathode Fall," Appl. Phys. Lett., 46, pp. 352-354, Feb. 1985.

[7] H. D. Hagstrum, "Auger Ejection of Electrons from Tungsten by Nobel Gas Ions," Phys. Rev., 104, pp. 317-318, 1956.

[8] H. D. Hagstrum, "Effect of Monolayer Adsorption on the Ejection of Electrons from Metals by Ions," Phys. Rev., 104, pp. 1516-1527, 1956.

[9] K. G. Emeleus, "The Negative End of Cold Cathode Glow Discharges," J. Phys. D: Appl. Phys., 14, 1981.

[10] A. E. D. Heylen, "Electrical Ionization and Breakdown of Gases in a Crossed Magnetic Field," IEE Proc., 127, pp. 221-244, 1980.

[11] J. J. Thomson, G. P. Thomson, Conduction of Electricity Through Gases, Volume II, Ionization By Collision and the Gaseous Discharge, London, Cambridge University Press, 1933.

[12] K. H. Schoenbach, T. J. Powers, S. T. Ko and V. K. Lakdawala, "The Effect of Transverse Magnetic Fields on Glow Discharges in Electronegative Gases," Proc. of the 1987 IEEE Conference on Plasma Science, (to be published).

[13] D. V. Turnquist, "Magnetic Field Control of a Gas Discharge Switch," Proc. of the Ninth Modulator Symposium, pp. 9.108-121, 1966.

[14] R. S. Willows, "On the Effect of a Magnetic Field on the Discharge Through a Gas," Philosophical Magazine, 6, pp. 250-260, 1901.

[15] R. L. Jepsen, "Magnetically Confined Cold-Cathode Gas Discharges at Low Pressures," J. of Appl. Phys., 32, pp. 2619-2626, 1961.

[16] M. A. Lutz and G. A. Hofmann, "The Gamitron - a High Power Crossed-Field Switch Tube for HVDC Interruption," IEEE Tran. on Plasma Science, PS-2, pp. 11-24, 1974.

[17] J. R. Cooper, K. H. Schoenbach and G. Schaefer, "Magnetic Control of Diffuse Discharges," IEEE Trans. on Plasma Science, PS-14, no. 4, Aug. 1986.

[18] L. E. Kline, D. K. Davies, C. L. Chen and P. J. Chantry, "Dielectric Properties for $SF_6$ and $SF_6$ Mixtures Predicted from Basic Data," J. Appl. Phys., 50, pp. 6789-6796, 1979.

[19] T. N. An, E. Marode and P. C. Johnson, "Monte Carlo Simulation of Electrons Within the Cathode Fall of a Glow Discharge in Helium," J. Phys. D: Appl. Phys., 10, 1977.

[20] J. R. Cooper, "Magnetic Field Control of Low Pressure Diffuse Discharges," Ph.D. Dissertation, Electrical Engineering Dept., Texas Tech University, 1986.

[21] B. E. Cherrington, Gaseous Electronics and Gas Lasers, New York, Pergamon Press, 1979.

[22] A. J. Davies, "Discharge Simulation," IEE Proc., 133, pp. 217-240, 1986.

[23] L. C. Pitchford, S. V. O'Neil and J. R. Rumble, "Extended Boltzmann Analysis of Electron Swarm Experiments," Phys. Rev. A, 23, pp. 294-304, 1981.

[24] K. H. Schoenbach, G. Schaefer, M. Kristiansen, H. Krompholz, D. Skaggs, and B. E. Strickland, "An E-beam Controlled Diffuse Discharge Switch," Proc. of the 5th IEEE Pulsed Power Conference, pp. 640-643, 1985.

[25] EG&G Electro-optics Div., Data Sheet T4000C-3, "Trigger Transformers and Chokes," 1981.

[26] A. D. White, "New Hollow Cathode Glow Discharge," J. of Appl. Phys., 23, 711-719, 1956.

[27] D. G. Samaras, Theory of Ion Flow Dynamics, New York, Dover Publications, Inc., 1971.

[28] H. Knoephel, Pulsed High Magnetic Fields:Physical Effects and Generation Methods Concerning Pulsed Fields up to the Megaoersted Level, New York, American Elsevier Publishing Co., 1970.